Central Burst and Alligatoring in Plane Strain Rolling

A thesis submitted
in partial fulfillment of the requirements
for the degree of

Master of Technology

by

Shaik Abdul Rajak

to the

Department of Mechanical Engineering
Indian Institute of Technology
Kanpur-208016, India
January, 2001

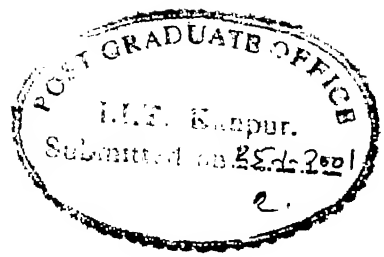

Certificate

This is to certify that the work contained in the thesis entitled **Central Burst and Alligatoring in Plane Strain Rolling** by *Shaik Abdul Rajak* is carried out under our supervision. This work has not been submitted elsewhere for a degree.

N. Venkat Reddy 25/01/2001

N. Venkat Reddy
Assistant Proffesor
Department of Mechanical Engineering
IIT Kanpur-208016

January, 2001

Acknowledgement

I feel immense pleasure and satisfaction by working with Dr. Reddy, the teacher with profound intellect and diverse interests, whose brilliant guidance throughout the period of my MTech thesis helped me to surpass all the obstacles smoothly. He introduced me to the subject of this thesis, guided and assisted me in difficult times and taught me the basics of research. His company not only enriches my knowledge but also widen my ways of thinking.

To my Parents and Teachers

Abstract

The occurrence of ductile fracture is the major limiting factor that determines the workability of cold bulk metal forming processes. Workability may be defined as the extent to which a material can be deformed without failure. Prediction of ductile fracture initiation will allow prior modification of the process which results in defect free final product with financial savings.

Two common defects which occur in rolling are central burst and split-ends. The consequence of these defects are not only limited to less productivity and also causes damage to the rolls and mill accessories. Recent literature [Zhu and Avitzur, 1988; Avitzur et al., 1988; Turckzyn and Malinowski, 1996] as well as the current practice in the rolling industry shows that the successful avoidance of defect is largely a matter of empirical practice or based on the upper bound based fracture criterion.

It is well known from literature [Dhar et al., 1996] that the ductile fracture occurs due to micro-void nucleation, growth and finally coalescence into micro-crack. Some experimental studies on extrusion and drawing revealed that the tensile triaxiality is the main factor contributing to the crack initiation. One can vizualize that the nature and magnitude of triaxiality generated in the deformation zone of plane-strain rolling process will be dependent on the various process variables. If the process variables are such that the tensile triaxiality arises in the deformation zone, then new micro-voids gets nucleated, existing voids grow and finally coalescence into micro-crack. Fracture occurrence can be prevented by choosing the proper process variables using mathematical modeling. Finite element method is the best modeling technique as it provides more accurate description of the deformation and stresses than other techniques. Hence, in the present work ductile fracture initiation is predicted using hydrostatic stress criterion [Reddy et al., 1996] and critical damage criteria [Dhar et al., 1996] along with the finite element results.

Force, torque and pressure predictions of the present model are in good agreement with the available experimental [Al-Salehi et al., 1973 and Shida and Awazuhara, 1973] and analytical [Dixit, 1997] results. Predictions of hydrostatic stress criterion for split ends are compared with the available experimental [Turckzyn and Malinowski, 1996]

results and they are in good agreement. Parametric study is carried out to study the influence of process variables on the boundary between safe and unsafe zones for defects. It is observed that with increase in roll radius or decrease in friction the safe zone in increasing.

Contents

List of Figures

List of Symbols

A	constant
A^e	area of the element e
$\bar{A}_n$	area fraction of voids
a	constant
a_i	constants
B	constant
$[B]$	spatial derivatives of shape functions matrix used in strain rate
b	constant
C	constant
$\dot{C}$	damage growth rate [Oyane et al., 1980]
C	damage variable [Oyane et al., 1980]
$\{C\}$	global damage variable vector [Oyane et al., 1980]
C_c	critical damage variable [Oyane et al., 1980]
C_D	constant
$\{C^e\}$	elemental damage variable vector [Oyane et al., 1980]
C_i	constants
D	damage variable [Dhar et al., 1996]
$\{D\}$	global damage variable vector [Dhar et al., 1996]
$\dot{D}$	damage growth rate [Dhar et al., 1996]
$\{D^e\}$	elemental damage variable vector [Dhar et al., 1996]
D_c	critical damage at fracture initiation [Dhar et al., 1996]
D_p	particle diameter
d_p	total number of pressure variables
d_s	particle spacing
E	modulus of elasticity
e	element number
F	constant
$\{F_C\}$	global RHS vector for damage evaluation [Oyane et al., 1980]
$\{F_D\}$	global RHS vector for critical damage evaluation [Dhar et al., 1996]
$\{F\}$	global RHS vector for rigid-plastic finite element method
$\{F_\varepsilon\}$	global RHS vector for strain evaluation
f	coefficient of friction
$\{f_x^b\}$	bounadry matrix
$\{f_y^b\}$	boundary matrix
$\{f_C^e\}$	elemental RHS vector for damage evaluation [Oyane et al., 1980]

$\{f_D^e\}$	elemental RHS vector for damage evaluation [Dhar et al., 1996]
G	shear modulus
h_0	initial thickness of strip
h_f	final thickness of strip
$[H]$	spatial derivatives of shape functions matrix
$I_i, \quad i=$ 1 to 4	functions
$\|J\|$	determinant of jacobian for area element
$[J]$	jacobian matrix for area element
$\|J_b\|$	determinant of jacobian for boundary element
k_s	constant
K	constant
$[K]$	global coefficient matrix for deformation analysis
$[K^e]$	elemental coefficient matrix for deformation analysis
$[K_C^e]$	elemental coefficient matrix for damage evaluation [Oyane et al. 1980]
$[K_D^e]$	elemental coefficient matrix for damage evaluation [Dhar et al. 1996]
$[K_{pv}^e]$, $[K_{vp}^e]$, $[K_{vv}^e]$	submatrices of $[K^e]$
$[K_\varepsilon^e]$	elemental coefficient matrix for strain evaluation
$[K_C]$	global coefficient matrix for damage evaluation [Oyane et al. 1980]
$[K_D]$	global coefficient matrix for damage evaluation [Dhar et al. 1996]
$[K_\varepsilon]$	global coefficient matrix for strain evaluation
$\{m\}$	constant vector
NBEX	number of boundary elements in x direction
NBEY	number of boundary elements in y direction
NEM	number of elements in the mesh
$\{N\}$	vector of biquadratic shape functions
N_i^p	bilinear shape functions
$\{N_b\}$	vector of boundary shape functions
N_i	biquadratic shape functions
$\{N_p\}$	vector of bilinear shape functions
$[N_v]$	biquadratic shape functions matrix for velocity approximation
n	constant
$\hat{n}$	unit normal vector
n_x, n_y	components of $\hat{n}$
P	power
p	hydrostatic stress
$\{p^e\}$	elemental hydrostatic stress vector
q_1	constant
$\dot{R}_{kv} : \quad k = 1, 2, 3.$	rate of change of void radii
R	roll radius
R_0	roll radius
R_{0h}	initial mean radii of the hole
R_{0v}	initial radius of the spherical void
R_h	current radii of the hole
$R_{iv} : \quad i = 1, 2, 3.$	principal radii of the ellipsoidal void
R_{mean}	mean radius of the void

$\%r$	percentage reduction in area
r_p	particle radius
S_F	surface of prescribed traction
S_u	remainder of surface
t	time
t_b	back tension per unit thickness
t_f	front tension per unit thickness
$\{t_x^b\}$	boundary elemental nodal traction vector of x component
$\{t_y^b\}$	boundary elemental nodal traction vector of y component
$t_i : i = x, y$	components of the stress vector
t_n	interfacial normal stress component
t_s	interfacial shear stress
T	roll torque
V_{entry}	entry velocity of the work
V_{exit}	exit velocity of the work
$\dot{V}_f$	rate of change of void volume fraction
$\dot{V}_{f-growth}$	rate of change of void volume fraction due to void growth
$\dot{V}_{f-nucleation}$	rate of change of void volume fraction due to void nucleation
$\{V^e\}$	elemental nodal velocity vector
V_f	void volume fraction
V_i	components of velocity vector
V_n	velocity normal to the interface
V_R	roll velocity
V_s	relative velocity tangent to the interface
V_x	x-component of velocity
V_y	y-component of velocity
$\{W\}$	global vector of weight functions in deformation analysis
$\{W^e\}$	elemental vector of weight functions in deformation analysis
$\{W_r^b\}$, $\{W_z^b\}$	boundary elemental nodal vectors of weight functions in deformation analysis
$\{W_C^e\}$	elemental nodal weight functions vector for damage [Oyane et al., 1980]
$\{W_D^e\}$	elemental nodal weight functions vector for damage [Dhar et al., 1996]
$\{W_p^e\}$	elemental nodal weight functions vector for hydrostatic stress
$\{W_v^e\}$	elemental nodal weight functions vector for velocities
$\{W_{\bar{\epsilon}}^e\}$	elemental nodal weight functions vector for strain
W_C	weight function for damage [Oyane et al., 1980]
W_D	weight function for damage [Dhar et al., 1996]
W_p	weight function for pressure p
W_x	weight function for velocity V_x
$\{W_v\}$	global weight functions vector for velocity
W_y	weight function for velocity V_y
$W_{\bar{\epsilon}}$	weight function for strain
$\{X\}$	global vector for nodal values of pressure and velocities
$\{X^e\}$	elemental vector for nodal values of pressure and velocities
$\{x^e\}$	elemental vector of x - coordinates

x_i	coordinate system
Y	elastic damage energy rate
$\{y^e\}$	elemental vector for nodal y-coordinates
α_b	bite angle
Γ_i	boundary i
γ	constant
δ_{ij}	Kronecker's delta
$\bar{\epsilon}$	generalized strain
$\{\dot{\epsilon}\}$	strain rate vector
$\{\dot{\epsilon}(W)\}$	vector containing derivatives of W_x, W_y
$\{\bar{\epsilon}\}$	global nodal vector of generalized strain
$\{\bar{\epsilon}^e\}$	elemental nodal vector of generalized strain
$\dot{\epsilon_{ij}}$	strain rate tensor
$\dot{\epsilon_{ij}}(W)$	tensor containing derivatives of W_x, W_y
$\dot{\bar{\epsilon}}$	generalized strain rate
$\dot{\epsilon}_k$	principal strain rates
ϵ_1^g	largest strain
ϵ_1	largest principal strain
ϵ_1^n	void nucleation strain
ϵ_a, ϵ_b	principal strain components
$\bar{\epsilon}_f$	generalized strain at which fracture occurs
ϵ_H	homogeneous strain
ϵ_v	volumetric strain
ϵ_{vf}	volumetric strain at fracture
$\bar{\epsilon}_i$	generalized strain at which fracture initiates
ζ, η	two dimensional natural coordinate
μ	Levy-mises coefficient
ν	Poisson's ratio and lode's variable
ξ	cross stream coordinate
ρ	mass density of the incompressible material
ρ_0	initial relative density of the porous material
ρ_r	relative density of porous material
σ_0	generalized stress at zero plastic strain
σ_1	maximum principal stress
σ_a, σ_b	principal stresses
σ_c	critical stress
σ_{ij}	stress tensor
$\bar{\sigma}$	generalized stress
$\bar{\sigma}^e$	effective generalized stress
$\bar{\sigma}_p$	generalized stress of the porous aggregate
σ_m	mean or hydrostatic stress
σ_{m_p}	mean or hydrostatic stress of the porous aggregate
σ_n	plastic constraint stress
σ_{xx}, σ_{yy}	stress components in x and y directions

σ_{xy}	shear stress component
$\{\sigma'\}$	nodal deviatoric stress vector
$\{\sigma'^{e}\}$	elemental deviatoric stress vector
τ	shear stress on surfaces of velocity discontinuity
ψ	stream function
Φ	plastic potential
ϕ	angle
Ω	region for deformation analysis

Chapter 1

Introduction and Literature Review

1.1 Introduction

Rolling is one of the most important process in metal working industry, and at the same time it is one of the oldest metal forming processes. According to some estimations, 90% [ASM handbook, vol. 14] of the steel stock is processed at least once in a rolling mill. Plane strain rolling is the process in which the sheet metal is squeezed through the gap between the two counter rotating work rolls to reduce the thickness as shown in the figure 1.1. The rolling process is one amongst the most often used, economical and most efficient techniques available, to produce sheets, plates and strips. Rolling process because of its versatility, efficiency and its high production rate playing an important role in the manufacturing industry. Primary objectives of the rolling process are to reduce the cross section of the incoming material and at the same time improve its properties and to obtain the desired shape.

Two common defects which occur in rolling are central burst (Fig. 1.2) and split ends (Fig. 1.3). The consequence of these defects are not only limited to less productivity and also causes damage to the rolls and mill accessories. In rolling process, without the complete knowledge of the influences of the variables such as friction conditions, material properties and workpiece geometry on the process mechanics, it will not be possible to predict and prevent the occurrence of defects, or to design the equipment adequately. It is almost impossible to find the exact analytical solutions of the equations governing real phenomenon by considering all aspects of process parameters and variables. Hence numerical simulation has become a major tool in modern metal forming research. Ability to predict the defect occurrence would allow prior modification of the process variables which eliminates the risk of failure occurrence, with obvious financial savings.

A number of approximate methods of analysis have been developed and applied to various metal forming processes. The most well known methods are the slab method, the slip line field method, upper bound method and more recently, the finite element method.

Critical review of literature [Avitzur et al., 1988; Turckzyn and Malinowski, 1996] on defects in rolling process shows that the successful avoidance of defect is largely a matter of empirical practice or based on the upper bound based fracture criterion which is not accurate as described in a later section. It is well known from the literature [Dhar et al., 1996] that the ductile fracture occurs due to micro-void nucleation, growth and finally coalescence into micro-crack. Many empirical criteria have been proposed to predict the occurrence of ductile fracture in various metal forming processes. From literature, it is evident that the empirical criteria have had only limited success [Clift et al. 1990]. Investigations on ductile fracture reveal that it occurs due to micro-void nucleation, growth and finally coalescence into micro-crack. Quite a few void growth models have been applied to predict ductile fracture in certain forming processes. The porous plasticity models, which incorporates both void nucleation as well as void growth, have also been used in some cases. The main draw back of these models is that they do not treat micro-crack initiation as a void coalescence phenomenon. There are no attempts to predict the fracture initiation in rolling process by using the more realistic fracture criteria developed on the basis of void nucleation, growth and coalescence [Dhar et al., 1996, and Thomason, 1990]. Hence, it is necessary to predict and prevent the fracture initiation in rolling process by choosing the proper process variables using more realistic fracture criteria.

The main aim of the present work is to predict and prevent the occurrence of central burst and alligatoring defects in plane strain rolling. Process modeling is performed using the finite element technique as it determines the process mechanics accurately compared to the other methods such as upper bound and slip-line methods. Two fracture criterion [Dhar et al, 1996 and Reddy et al., 1996] are used along with the finite element results to predict the fracture occurrence in plane strain rolling process. Comprehensive parametric study is carried out to study the influence of process variables on the process parameters and defect occurrence.

1.2 Literature Review

1.2.1 Deformation Analysis

Rolling process has been analyzed extensively by the slab method, slip-line field method, upper bound method and the finite element method.

1.2.1.1 Slab method

The slab method is known to be developed by Sachs and Siebel. In this method, the deformation zone is divided into a finite number of 'slab' elements and an equilibrium equation for a typical slab is solved, subject to the given stress boundary conditions. The distribution of contact pressure at the tool-work interface can be obtained based on a simplification of stress state. The assumptions on which this method is developed are:

- The stresses on a slab surface, perpendicular to the flow direction, are working in principal directions and they are not permitted to vary on this surface.
- Frictional stresses do not effect the internal stress distribution.

Many researchers have been developed mathematical models to study rolling problem, using slab method. Starting from the pioneering work of von Karman [1925], Orowan [1943], Bland and Ford [1948], Bland and Sims [1953], Ford and Alexander [1963], Tselikov [1939], Stone [1953], Robert [1967] and Lenard and Roy Choudhuri [1984] and recently by Surya Narayana [1998]. A brief comparison of these models is given below.

Orowan [1943], Bland and Ford [1948], Sims [1954] considered the roll contour to remain circular after the deformation and that the radius of curvature becomes larger than the original roll radius. They used Hitchcock's [1935] method to calculate the deformed roll radius. Roy Choudhuri and Lenard [1984] pointed out that Hitchcock's formula does not predict the deformed roll shape accurately and proposed an approximate method to calculate the same.

Pietrzyk and Lenard [1991] compared the predictive capabilities of the six [Orowan, 1943, Sims, 1954, Bland and Ford, 1948, Ford and Alexander, 1963, Tselikov, 1939, Roy Choudhuri, 1984] models and along with experimental data. They observed that the Orowan's [1943] technique proved to be reasonable in predicting roll forces and roll torques. The Bland and Ford [1948] analysis gave results very close to that of Orowan [1943]. They also observed that the inclusion of the experimentally determined data concerning friction

at roll strip interface enhances the ability of the model of Roy Choudhuri and Lenard [1984] in calculation of the roll forces.

Lin et al. [1996] compared three one dimensional models qualitatively [Robert's, 1967, Stone, 1953, Bland and Ford, 1948]. They reported that the Stone's [1953] model, using Hitchock's [1935] deformed radius equation gives a good estimation of roll separating force for strip reductions larger than 3 percent and less than 5 percent. They observed that when compared with other models, it is not recommended for reductions less than 3 percent. They also observed that Robert's [1967] model using Robert's [1967] deformed radius equation, can be used for predicting the roll separating force while rolling very thin strip with thickness less than 0.5 mm and reductions less than 3 percent.

From the above discussion, it can be said that Robert's [1967] method is efficient when compared with other methods as it considers strain rate effects, which other methods does not consider. The reason for this is the presence of the gradient of flow stress in the equilibrium equations in the other one dimensional methods mentioned above. Recently Surya Narayana [1998] developed a one-dimensional mathematical model, in which he eliminated the gradient of flow stress from the governing equations to incorporate the realistic material properties. The influence of strain rate in prediction of roll forces and roll torques was reported by Tseng et al. [1998].

1.2.1.2 Slip-line method

Slip line method is used to obtain the stress field in a forming problem by constructing slip lines. Originally, the method was proposed for strain analysis of rigid perfectly plastic materials. However, lately there have been some attempts to expand the method to axisymmetric problem as well as to incorporate strain hardening.

Some researchers have analyzed the rolling process by slip-line method. Firbank and Lancaster [1965] proposed a slip line field for cold rolling with slipping friction. Their solution is for small rolls and a pass reduction of 20 percent. In slip line solutions peak pressures occur at the entry and exit, and there is considerable pressure drop some where in between those two points. New slip line solution for compression and rolling with slipping friction was presented by Collins [1969].

1.2.1.3 Upper bound method

The upper bound method is a technique for determining an over estimation of the exact load, obtained from an assumed kinematically admissible velocity field which satisfies the

conditions of incompressibility and velocity boundary conditions. An extensive literature exists on upper bound analysis of metal forming processes and have been reviewed by many researchers [Avitzur, 1980, 1983; Bramley and Osman, 1992; Hill, 1950; Johnson and Mellor, 1973; Kudo, 1985; and Thomsen et al., 1965] and particularly on rolling by Avitzur [1988]. The upper bound method requires the guessing of admissible velocity fields, among which best one is chosen by minimizing the total energy. Information leading to a good selection of velocity fields come from experimental evidence and experience.

Avitzur's [1964] upper bound solutions gives an expression for roll torque and the position of the neutral point, but does not provide roll force and pressure distribution which are important design parameters. The major difficulty in using upper bound method is the selection of kinematically admissible velocity field since the accuracy of the solution depends on how close the assumed velocity field is, to the actual one. For the cases in which roll flattening is significant and may affect torque, one has to compute roll force by some other method and calculate deformed radius of roll which is then to be substituted in the expression of the torque developed by Avitzur [1964].

Avitzur and Pachla [1986] developed a upper bound approach to plane strain deformation of a rigid, perfectly plastic material in rolling process. They divided the deformation region into a finite number of rigid triangular bodies that slide with respect to one another. Neighboring rigid body zones are analyzed in specific cases where the zones are (1) both in rotational motion, (2) one in linear and another in rotational motion, and (3) both in linear motion. Specific equations are presented that describes surface of velocity discontinuity (shear boundaries) between the moving bodies, and the velocity discontinuities and shear power losses for each of the three cases. Avitzur and Pachla [1986a] applied these equations drawing, extrusion and rolling. And explicit equations are developed to calculate the surfaces of velocity discontinuity (shear boundaries), velocity discontinuities, and the upper bound on power for these processes.

Avitzur et al. [1987] analyzed the strip rolling using the upper bound technique. The general solution given in Avitzur and Pachla [1986] is applied here to the problem of strip rolling. Two triangular velocity fields, one with triangles in linear rigid body motion and the other with triangles in rotational rigid body motion are developed. The total power is determined as a function of the four independent process parameters namely relative thickness, reduction, friction and net front-back tension.

1.2.1.4 Finite Element Analysis

Slab, slip-line and upper bound methods are useful in making the approximate predictions for the forming loads, the overall geometry changes in the deforming work pieces, the qualitative modes of metal flow and optimal process conditions. However, accurate determination of the effect of various process parameters on the metal flow became possible only after the finite element method was introduced into the analysis of the metal forming processes. In finite element method, the domain of interest is divided into a number of suitable elements and the governing differential equations of the system are reduced to algebraic equations by using appropriate approximations for the field variables over the elements. Almost all metal forming processes have been analyzed by the finite element method due to its ability to handle a wide class of boundary value problems without restriction on the work piece geometry. This can be achieved by selecting a proper mesh. Several review papers and text books have appeared outlining the state of art of the finite element analysis of metal forming processes [Altan and Knoerr, 1992; Cser et al., 1993; Hartley et al., 1992; Herrmann, 1994; Altan and Vazquez, 1997].

Rigid-Plastic Finite Element Analysis

The use of elasto-plastic formulation involves certain numerical difficulties. Since elastic effects are usually small, it is desirable to idealize the material as rigid-plastic, if it helps in avoiding the numerical difficulties. Zienkiwicz et al. [1978] considered the rolled material to be rigid-visco-plastic and incompressible. They simulated the friction at the roll-strip interface by introducing a thin layer of elements whose yield strength is assumed to depend on the coefficient of friction and mean stress. Mori et al. [1982] assumes that the rolled strip is made of a rigid-plastic, slightly compressible material. Using a constant frictional coefficient and rigid rolls they reported good agreement between the predicted and observed front end shapes of rolled aluminium strips. In their formulation, neutral point was determined by minimizing a certain functional. Li and Kobayashi [1982; 1984] also assumes the existence of rigid-plastic materials and rigid rolls but they modeled the neutral point using the velocity dependent frictional stress. The authors included a comparison of their predictions with the results of Al-Salehi et al. [1973], and Shida and Awazuhara [1973]. In acknowledging that some discrepancies do exist, they attributed them to their use of rigid rolls and some uncertainty in modeling interfacial friction.

Prakash et al. [1995] presented a FEM formulation in which the neutral point is found iteratively from the condition that the interfacial shear stress changes its sign at the neutral

point. This formulation does not incorporate roll deformation. Recently, Dixit and Dixit [1996] presented a rigid-plastic finite element formulation, to calculate the residual stresses. They applied fuzzy set theory to calculate material properties and friction coefficient. They applied this fuzzy set theory to avoid uncertain behavior in these parameters. They included anysotrophy in formulation, and also considered roll deformation. The front and back tensions also included in this formulation.

Elasto-Plastic Finite Element Analysis

Eulerian elasto-viscoplastic formulations have been reported by many authors. Dawson and Thompson [1978] have developed 'initial stress rate' method. In this approach, the stress and velocity fields associated with the convective terms are assumed known and placed on the right-hand side of the finite element equations for momentum. An iterative procedure is then used during which these terms are corrected until there is no discrepancy between the new stress distribution and the precious one. The stress values are corrected until there is no discrepancy between the two successive iterations. Shimazaki and Thompson [1981] used the mixed formulation to solve for velocity, pressure and stress simultaneously. In their method, they decoupled the momentum and continuity equations from the constitutive equation. The former set was used to obtain velocity and pressure with stress assumed constant. the latter set was used to obtain stress with velocity and pressure held constant. Iterations between these two sets were done until convergence. Thompson and Berman [1984] employed the procedure developed by Shimazaki and Thompson [1981] for the analysis of plane-strain rolling. However, rate of convergence was slow and results presented are without getting full convergence. Effective stress contours are plotted, but individual stress components have not been presented. Thompson and Yu [1990] have presented a flow formulation to solve the rate equilibrium equation, in their steady state form, for velocity and stress. The authors have used the formulation for the analysis of strip drawing for a perfectly plastic material. It is noted that the rate of convergence deteriorates as the inelastic response becomes large. Effective stress contours are plotted without getting full convergence. No result is presented for residual stress distribution.

Maniatty et al. [1991] have proposed an eulerian elasto-visco-plastic formulation in which the kinematics consists of a multiplicative decomposition of the deformation gradient into elastic and plastic components. They used Hart's constitutive model, which contains an internal scalar variable, for analyzing plane strain rolling and extrusion processes. The system of equations is highly ill-conditioned and the algorithm lacks stability as the material becomes less rate sensitive. Maniatty [1994] modified the above formulation by using the

discontinuous pressure field by eliminating the pressure as a primary variable. He adjusted the mesh to align with the streamlines so that the constitutive equations can be integrated from node to node along the mesh lines and analyzed the rolling process to show the effectiveness of the algorithm.

Malinowski and Lenard [1993] presented an elasto-plastic finite element formulation using the Prandtl-Reuss constitutive relations which was applicable for steady-state plane strain problems. In this formulation, the velocity field is first determined by minimizing the total power. The stresses are then obtained by integrating the Jaumann stress rate along the pathlines and minimizing a functional which relates the Jaumann rate to the material derivative of the stress using the finite element method. Pathline integration gives unrealistic results due to non-satisfaction of the equilibrium condition. In the finite element procedure of finding stresses, they used two types of shape functions (parabolic and Hermitian) and the results differ significantly from each other. The formulation assumed the poisson's ratio to be a continuous material function defined for both elastic and elasto-plastic behaviors. Malinowski [1993] used the methodology developed by Malinowski and Lenard [1993] for determining residual stress distribution in plane strain cold rolling.

Recently, Dixit and Dixit [1997] presented elasto-plastic formulation for rolling problem. The formulation presented here is similar (but not exactly the same) to that of Shimazaki and Thompson [1981], Thompson and Berman [1984], the main difference being in the constitutive equations. In Shimazaki and Thompson [1981], Thompson and Berman [1984], they considered whole domain as elasto-plastic and the same constitutive equation is used throughout the domain, where as in Dixit and Dixit [1997] different constitutive relations are used for the elastic and elasto-plastic regions.

1.2.2 Ductile Fracture Criteria

Ductile fracture is often a limiting factor in many metal forming processes. It is well known that ductile fracture occurs due to micro-void nucleation, growth and finally coalescence into micro crack. Many ductile fracture criteria have been proposed and applied to predict ductile fracture in plastically deforming metals including metal forming processes. This section reviews some of the published ductile fracture criteria.

The published ductile fracture criteria can be broadly classified into two groups. They are

- Models based on microscopic observations about void nucleation, growth and coalescence

- Empirical and semi-empirical models

Three broad approaches have emerged which try to predict ductile fracture (micro-crack initiation) on the basis of void nucleation, growth and coalescence. They are

- Models based on porous plasticity
- Models of void nucleation, growth and coalescence
- Continuum damage mechanics models

1.2.2.1 Models of Porous Plasticity

In these models, the material with voids is idealized as porous material. Thus, its constitutive equation is derived form the plastic potential of porous materials. In a porous plastic material, there is a possibility of dilatation because of which the yield surface does not remain an infinitely long cylinder like that of an incompressible material but is capped by elliptical surfaces.

Gurson's Model

Based on the Berg's [1970] model of dilatational plasticity, Gurson [1977] proposed a plastic potential function for a porous solid with randomly distributed voids of volume fraction V_f in the form

$$\Phi = \frac{\bar{\sigma}_p^2}{\bar{\sigma}^2} + 2V_f \cosh\left(\frac{3\sigma_{m_p}}{2\bar{\sigma}}\right) - (1 + V_f^2) = 0 \tag{1.1}$$

where $\bar{\sigma}_p$ and σ_{m_p} are the generalized and hydrostatic stresses of the porous aggregate and $\bar{\sigma}$ is the generalized stress of the void free (incompressible) matrix.

In this model, the growth rate of void volume fraction is considered partly due to the growth of the existing voids and partly due to the nucleation of new voids. i.e.,

$$\dot{V}_f = \dot{V}_{f-growth} + \dot{V}_{f-nucleation} \tag{1.2}$$

The rate of change of the void volume fraction due to the growth of existing voids is related to the mean strain rate $\dot{\epsilon}_{ii}$ by the relation

$$\dot{V}_{f-growth} = (1 - V_f)\ \dot{\epsilon}_{ii} \tag{1.3}$$

In general, void nucleation rate depends on both the generalized strain rate as well as the rate of increase of hydrostatic stress. In this model, void nucleation rate is assumed to depend only on the generalized strain rate by the relation

$$\dot{V}_{f-nucleation} = A\dot{\bar{\epsilon}} \tag{1.4}$$

where A is a constant.

Gurson's criterion [1977] was modified by Tvergaard [1981] and Needleman and Tvergaard [1984] by introducing some constant (q_1) to bring the predictions of the model into closer agreement with numerical analysis of a periodic array of voids. The modified criterion is given by

$$\Phi = \frac{\bar{\sigma}_p^2}{\bar{\sigma}^2} + 2q_1 V_f \cosh\left(\frac{3\sigma_{m_p}}{2\bar{\sigma}}\right) - (1 + (q_1 V_f)^2) = 0 \tag{1.5}$$

where q_1 is a constant.

In this model, ductile fracture is regarded as the result of an instability in the dilatational plastic flow field localized in a band (called the shear band). The fracture criterion is represented as a graph of critical localization strain versus the critical void volume fraction with strain hardening exponent as a parameter.

Oyane's Model

Oyane [1972] and Oyane et al. [1980] used the plasticity theory for porous materials to propose a ductile fracture criterion indicating that micro crack initiates whenever the volumetric strain reaches a material dependent critical value. For pore free materials, assuming that the material obeys porous plasticity equations after the initiation of voids, Oyane obtained the criterion for ductile fracture as

$$\int_0^{\epsilon_{vf}} f_\rho^2 \rho_r^{2n-1} d\epsilon_v = C \tag{1.6}$$

where f_ρ is a function of relative density ρ_r which is defined as the ratio of the apparent density of the porous material to the density of the pore free matrix, ϵ_{vf} is the volumetric strain at fracture and n and C are constants. The constant C is given by

$$\int_{\bar{\epsilon}_i}^{\bar{\epsilon}_f} \left(1 + \frac{\sigma_m}{A\bar{\sigma}}\right) d\bar{\epsilon} = C \tag{1.7}$$

where $\bar{\epsilon}_i$ is the generalized strain at which voids get initiated, $\bar{\epsilon}_f$ is the generalized strain at which fracture occurs and A is a material constant. By assuming that $\bar{\epsilon}_i = 0$, the above criterion reduces to a simple form

$$\int_0^{\bar{\epsilon}_f} \left(1 + \frac{\sigma_m}{A\bar{\sigma}}\right) d\bar{\epsilon} = C \tag{1.8}$$

For porous materials, they modified the criterion by including the relative density term into the integral. Thus,

$$\int_0^{\bar{\epsilon}_f} \left(1 + \frac{\sigma_m}{A\rho_r^n\bar{\sigma}}\right) d\bar{\epsilon} = C\rho_0^B \tag{1.9}$$

Here $\rho_r^n\bar{\sigma}$ is the generalized flow stress of the porous material, B is a constant and ρ_0 is the initial relative density of the porous material. A method for estimating values of the material constants using the compression test has been provided by them.

The major limitation of the above two criterion is that they do not model ductile fracture (i.e., micro-crack initiation) as a void coalescence phenomenon.

1.2.2.2 Models of Void Nucleation, Growth and Coalescence

The void nucleation model of Goods and Brown [1979], the growth models of McClintock [1968] and Rice and Tracey [1969] and void coalescence model of Thomason [1990] along with some additional models on void nucleation and growth are discussed in this section.

Models on Void Nucleation

Goods and Brown [1979] developed a stress based void nucleation model based on condition that the voids nucleate by decohesion of particles whenever the normal stress reaches a critical value (σ_c) at the particle/matrix interface. They obtained a relation between the void nucleation strain (ϵ_1^n) and hydrostatic stress (σ_m) as

$$\epsilon_1^n = Kr_p(\sigma_c - \sigma_m)^2 \tag{1.10}$$

where K is a material constant dependent on the particle volume fraction and r_p is the particle radius. Experiments on $Fe - Fe_3C$ system [Goods and Brown, 1979] confirm the linear relationship between the nucleation strain and particle radius. This relation is for small spheroidal particles of radius less than or equal to 1μm.

For large size particles, the approximate analysis of Argon and Im [1975] gives the condition for the void nucleation by decohesion as

$$\bar{\sigma} + \sigma_m = \sigma_c \tag{1.11}$$

For a given problem, this condition can be expressed in terms of the nucleation strain. Note that this relation is independent of particle radius.

Gurland [1972] proposed a nucleation model based on the experiments conducted by him on 1.05%C spheroidal steel. Experimental observations reveal that the void nucleation occur by cracking of cementite particles. Voids nucleate at all strain levels depending on the size, shape and orientation with the maximum principal stress direction. It is observed that the volume fraction of broken particles is a linear function of the plastic strain.

Void Growth Models

Once the nucleation of micro-void takes place either by decohesion or cracking of a secondary particle or inclusion, the resulting stress free surface of the void produces a localized stress and strain concentration in the plastically surrounding matrix. With continuing plastic flow of the matrix, the void undergoes volumetric growth and change of shape. Some of the published void growth models are discussed here.

McClintock [1968] proposed a void growth model for two-dimensional plane strain problems considering a single elliptic void. He assumed that the major and minor axes of the void coincide with the principal stress directions. He obtained the following closed form expression for void growth in a rigid work-hardening material whose generalized stress relation is $\bar{\sigma} = K\bar{\epsilon}^n$:

$$ln\frac{R_h}{R_{0h}} = \frac{\sqrt{3}\bar{\epsilon}}{2(1-n)}\sinh\frac{\sqrt{3}(1-n)}{2}\frac{\sigma_a+\sigma_b}{\bar{\sigma}} + \frac{\epsilon_a+\epsilon_b}{2} \tag{1.12}$$

where R_h and R_{0h} are the current and initial mean radii of the hole respectively, σ_a and σ_b are the principal stress and ϵ_a and ϵ_b are the principal strain components along the major and minor axes respectively. Fracture was assumed to occur at the point where a growing void touches the cell boundary. Dung [1992a, 1992b] modified and extended McClintock's model [1968] to analyze the growth of circular/ellipsoidal void in three-dimensional problems.

Rice and Tracey [1969] considered a single spherical void of initial radius R_{0v} in a remote uniform strain rate field $\dot{\epsilon}_{ij}$ and remote stress field σ_{ij} in a plastic material. They obtained the following expression for the rate of change of the radii($\dot{R}_{kv}$) of the void in the principal strain rate directions:

$$\dot{\bar{R}}_{kv} = \{(1+F)\dot{\epsilon}_k + \dot{\bar{\epsilon}}H\}R_{mean} \tag{1.13}$$

where

F = $\frac{2}{3}$ for linear hardening and for low values of σ_m for non hardening

= 1 for high values of σ_m for non hardening

H = $0.75\frac{\sigma_m}{\bar{\sigma}}$ for linear hardening

= $0.558 \sinh \frac{3}{2}\frac{\sigma_m}{\bar{\sigma}} + 0.008\nu \cosh \frac{3}{2}\frac{\sigma_m}{\bar{\sigma}}$ for non hardening,

R_{mean} = generalized strain rate

$\dot{\bar{\epsilon}}$ = principal strain rates

ν = $-\frac{3\dot{\epsilon}_2}{\dot{\epsilon}_1 - \dot{\epsilon}_3}$, Lode variable.

Note that an initial spherical void grows into an ellipsoidal void of principal radii R_{1v}, R_{2v} and R_{3v}. Thomason [1990] integrated the above equation by assuming that the principal axes of strain rates remain fixed in direction throughout the strain path and obtained the following expressions for the principal radii of the void:

$$R_{1v} = \left(A + \frac{3B(1+\nu)}{2\sqrt{\nu^2+3}}\right) R_{0v} \tag{1.14}$$

$$R_{2v} = \left(A - \frac{B\nu}{\sqrt{\nu^2+3}}\right) R_{0v} \tag{1.15}$$

$$R_{3v} = \left(A + \frac{B(\nu-3)}{2\sqrt{\nu^2+3}}\right) R_{0v} \tag{1.16}$$

where

$$A = exp\frac{2\sqrt{\nu^2+3}}{3+\nu} H\epsilon_1^g$$

$$B = \frac{1+F}{H}(A-1)$$

and ϵ_1^g is the integral of the largest principal strain rate. Thomason [1990] used the above expressions in the derivation of the void coalescence condition.

For an array of void nucleating particles of diameter D_p and spacing d_s, setting the initial void radius as $D_p/2$, eqns. (1.12) and (1.13) leads to the following expression for fracture strain:

$$\bar{\epsilon}_f = \frac{ln\,(d_s/D_p)\,(1-n)}{sinh\,[(1-n)(\sigma_a+\sigma_b)/(s\bar{\sigma}/\sqrt{3})]} \qquad \text{[McClintock, 1968]} \tag{1.17}$$

$$\bar{\epsilon}_f = \frac{ln\,(d_s/D_p)}{0.28\,\exp\,(1.5\sigma_{kk}/\bar{\sigma})} \qquad \text{[Rice and Tracey, 1969]} \tag{1.18}$$

Some research workers have used the above expressions for the prediction of ductile fracture with the help of experimentally determined parameters. The major limitations of the approach are that it ignores the effects of void nucleation (as the expressions are derived from a pre-existing finite size void) and void coalescence. Thus, $\bar{\epsilon}_f$ is usually overestimated.

Void Coalescence Model

Thomason [1990] modeled void coalescence phenomenon as plastic instability due to necking of the inter void matrix. The sufficient condition for plastic instability of the inter-void matrix, as given by him, is

$$\sigma_n \bar{A}_n - \sigma_1 = 0 \tag{1.19}$$

where $\bar{A}_n$ is the area fraction of the inter-void matrix perpendicular to the direction of maximum principal stress σ_1 and σ_n is the plastic constraint stress. He considered a geometrically equivalent square prismatic void and used the upper bound method to obtain an expression for the plastic constraint stress in terms of the void dimensions, inter-void spacing and the yield stress.

Thomason's Fracture Criterion

Thomason [1990] combined the results of Goods and Brown [1979] on void nucleation, Rice and Tracey [1969] on void growth and his own on void coalescence to arrive at a fracture criterion. He used expressions (eqn. 14 to 16) for the void dimensions to express the void coalescence condition (eqn. 19) in terms of the void growth strain ϵ_1^g and the hydrostatic stress σ_m. By superposing this condition on the void nucleation relation (eqn. 10), he obtained the fracture criterion as a graph of fracture strain ($\bar{\epsilon}_f = \epsilon_1^n + \epsilon_1^g$) versus the triaxiality (i.e., the ratio of hydrostatic stress to the generalized stress).

The main drawback of this approach is the use of expressions (eqn. 14 to 16) for void growth. There expressions are based on integration procedure which assumes that the principal directions of strain rate remain fixed throughout the strain path. This is, in general, true only of the case of small strain and rotation.

1.2.2.3. Continuum Damage Mechanics Models

In these models, material behavior is represented by a plastic potential which includes damage as an internal variable. The damage variable quantifies the intensity of voids, which can be identified as either the void volume fraction or the area void fraction. The basis of

continuum damage mechanics models rests on the theory of continuum thermodynamics. In this section some of the continuum damage mechanics models are discussed.

Lemaitre [1985] proposed a continuum damage mechanics model for void growth in elasto-plastic material with area void fraction as the damage variable using concepts of effective stress and strain equivalence. His model is based on a simple damage growth law in which the damage rate is linearly dependent on the plastic strain and the thermodynamic force corresponding to the damage. It does not account for void nucleation. Note that, as far as void coalescence is concerned, it has to be incorporated as an additional condition in terms of the continuum parameters. This condition, which serves as a fracture criterion, has to be based on an appropriate micro model. Thomason's limit load model seems to be a good candidate for this purpose.

More recently Dhar [1995] and Dhar et al. [1996] extended Lemaitre's [1985] continuum damage mechanics model to incorporate a damage growth law which accounts for both the void nucleation as well as void growth. The law is based on the experimental results of Le Roy et al. [1981]. They also modified Thomason's [1990] void coalescence condition to make it suitable for the case of large strain and/or rotation. They combined the extended continuum damage mechanics model and modified void coalescence condition to arrive at a criterion for prediction of micro crack initiation. The salient features of the above approach are discussed below.

In this model, damage D is identified as an area void fraction at a point in a plane. Thus, it is defined by

$$D = \frac{\Delta A_v}{\Delta A} \tag{1.20}$$

where ΔA is the infinitesimal area around the point in some plane and ΔA_v is the area of the voids in the plane containing ΔA. The conjugate variable corresponding to D is -Y, the rate at which the elastic energy release during the damage growth at constant stress. For an isotropic material, -Y is given by [Lemaitre, 1985]

$$-Y = \frac{\bar{\sigma}^2}{2E(1-D)^2} f(\frac{\sigma_m}{\bar{\sigma}}) \tag{1.21}$$

where

$$f(\frac{\sigma_m}{\bar{\sigma}}) = \frac{2(1+\nu)}{3} + 3(1-2\nu)\frac{{\sigma_m}^2}{\bar{\sigma}} \tag{1.22}$$

Here, E is the Young's modulus, ν is the Poisson's ratio and $\frac{\sigma_m}{\bar{\sigma}}$ is called the triaxiality. the damage growth law is given by

$$\dot{D} = C_D\dot{\bar{\epsilon}} + (a_1 + a_2 D)(-Y)\dot{\bar{\epsilon}} \tag{1.23}$$

where a_1, a_2 and C_D are material constants. Here the first term, which is independent of -Y, represents the damage evolution due to void nucleation while the second term, which is dependent on -Y, represent the evolution of damage due to void growth. For SAE 1090 steel, Dhar et al. [1995] determined the constants fitting eqn. (1.23) through the experimental results of Le Roy et al. [1981]. They obtained the following values:

$$C_D = 1.898X10^{-2} \tag{1.24}$$

$$a_1 = 9,8X10^{-4}\ MPa^{-1} \tag{1.25}$$

$$a_2 = 1.84\ MPa^{-1} \tag{1.26}$$

While getting these constants, they used Bridgman's relation [1964] to express the triaxiality as a function of strain.

Dhar et al. [1996] used finite strain expressions for the void dimensions and inter-void spacing to express Thomason's void coalescence criterion (eqn. 1.19) in the following form:

$$\sigma_1 \left[0.1 + \frac{1.2}{\{1 - exp(-\bar{\epsilon}/2)\}^{0.5}}\right] exp(-\bar{\epsilon})\ \bar{\sigma} = 0 \tag{1.27}$$

where $\bar{\epsilon}$, the generalized strain, is the integral of $\dot{\bar{\epsilon}}$ along the path lines. To find the critical value of damage parameter (D_c), they applied this criterion to various geometries and loading conditions using the elasto-plastic finite element analysis. They observed that D_c is independent of geometry or loading and here that can be used as a material property for the prediction of micro-crack initiation. They reported that the value of D_c is 0.05 for SAE 1090 steel.

1.2.2.4. Empirical and Semi-Empirical Models

In the absence of reliable quantitative models for incorporating the phenomena of void nucleation, growth and coalescence in materials undergoing large plastic deformation in metal forming processes, many empirical relations based on some phenomenological models have been proposed. This section reviews some of them.

Frudenthal's Model

Freudenthal [1950] postulated that generalized plastic work per unit volume is the critical parameter and is expressed as

$$\int_0^{\bar{\epsilon}_f} \bar{\sigma} d\bar{\epsilon} = C_1 \tag{1.28}$$

Cockcroft - Latham's Model

Cockcroft and Latham [1968] modified the generalized plastic work criterion to take care of the effects of change in the neck geometry which is observed in tensile tests. The criterion is given by

$$\int_0^{\bar{\epsilon}_f} \bar{\sigma} \frac{\sigma_1}{\bar{\sigma}} d\bar{\epsilon} = \int_0^{\bar{\epsilon}_f} \sigma_1 d\bar{\epsilon} = C_2 \tag{1.29}$$

Here σ_1 is the maximum normal stress.

Oh's Model

Oh et al. [1979] modified Cockcroft and Latham criterion [1968] by considering the relation of the maximum tensile stress to the generalized stress. This criterion is expressed as

$$\int_0^{\bar{\epsilon}_f} \frac{\sigma_1}{\bar{\sigma}} d\bar{\epsilon} = C_3 \tag{1.30}$$

The main drawback of the above three criteria is that the effect of hydrostatic stress is not considered.

Brozzo's Model

Brozzo et al. [1972] proposed an empirical modification of Cockroft and Lathat's model to consider the effect of hydrostatic stress explicitly. The criterion considers Hydrostatic stress is given by

$$\int_0^{\bar{\epsilon}} \frac{2\sigma_1}{3(\sigma_1 - \sigma_m)} d\bar{\epsilon} = C_4 \tag{1.31}$$

Norris's Model

Norris et al. [1978] developed a fracture criterion based on their experimental results and finite difference results of several test geometries and expressed it as

$$\int_0^{\bar{\epsilon}_f} \frac{1}{(1 - C\sigma_m)} d\bar{\epsilon} = C_5 \tag{1.32}$$

where C is a constant.

In the above equations $C_1, \ldots C_5$ are the critical material dependent values accumulated over the strain path to fracture.

1.2.2.5 Hydrostatic Stress Criterion

Some experimental studies on extrusion revealed that the tensile triaxiality is the main factor contributing to the crack initiation. One can vizualize that the nature and magnitude of triaxiality generated in the deformation zone of plane-strain rolling process will dependent on the various process variables. If the process variables are such that the tensile triaxiality arises in the deformation zone, then new micro-voids gets nucleated, existing voids grow and finally coalescence into micro-crack. The work of Clift et al. [1990] shows that the value of hydrostatic stress at fracture initiation in extrusion is close to zero. Based on this observations, Reddy et al. [1996] proposed a simple criterion given as
'whenever hydrostatic stress at a point on the centerline in the deformation zone becomes zero and is compressive elsewhere, there is fracture initiation leading to central burst'.
One of the main advantage of this criterion is that it does not involves any critical material parameter which needs to be determined experimentally.

1.2.3 Defects in Rolling Process

Different type of defects are observed in industrial metal forming processes which have been tabulated by Johnson and his co-workers [Johnson and Mamalis, 1977; Mamalis and Johnson, 1987; Johnson, 1991]. Two common defects which will occur in rolling process are central burst and alligatoring (split-end) [Avitzur et al., 1988].

Criterion for prevention of central bursting and split ends in plane-strain rolling were derived by Avitzur and his coworkers [Zhu and Avitzur, 1988; Avitzur et al., 1988] by extending an earlier upper bound solution [Avitzur, 1964] for strip rolling of a rigid perfectly-plastic Mises material. Their criterion for defect prediction is that for a given set of process parameters the power consumption for defect-free flow is higher that that for a defect flow. Turckzyn and Malinowski [1996] used the same criterion as above to predict the central burst and split ends in rolling. They also conducted experiments to predict occurrence of split end defects in rolling.

It is well known that the tensile triaxiality is the main factor contributing to the crack initiation in metal forming processes. Note that, all the attempts made for predicting the central bursting and split ends in rolling [Zhu and Avitzur, 1988; Avitzur et al., 1988; Turckzyn and Malinowski, 1996] are based on kinematically admissible velocity field (Upper bound analysis) but not on the basis of statically admissible velocity field. The circumstances which may lead to deduction of a greater driving force for the process involving a defect must arise because the upper bound to the driving force with a defect is sufficiently

above the correct value to exceed the greater correct value corresponding to defect-free product. Use of lower bound theorem [Lee and McMeeking, 1978] indicates that the actual driving force for the cracked workpiece provides a lower bound for the uncracked case. Thus the correct driving force for the uncracked case is always greater than or equal to that for the cracked case. Hence, the inequality in the defect prediction criterion used by Avitzur and his coworkers [Zhu and Avitzur, 1988 and Avitzur et al., 1988] and Turckzyn and Malinowski [1996] implies that the defect always occurs.

1.3 Scope and Objective of the Present Work

Critical literature review reveals that there have been very few attempts to predict the occurrence of central burst and alligatoring in rolling. Recent literature [Avitzur et al., 1988 and Turckzyn and Malinowski, 1996] as well as the current practice in the rolling industry shows that the successful avoidance of defect is largely a matter of empirical practice or based on the upper bound based fracture criterion. Present work aims at prediction and prevention of central bursting and split ends in plane-strain rolling by choosing the proper process variables through finite element based process modeling as it determines the process mechanics accurately compared to other methods such as upper bound method and slip line method. The various rolling process variables which will effect the defect occurrence are relative reduction in thickness, front and back tensions, friction, material properties, roll velocity and radius.

The main objective of the present work is to predict and prevent the occurrence of central burst and alligatoring in rolling. The above objective is achieved through the following steps:

- Development of Eulerian rigid-plastic finite element formulation with isotropic hardening and implementation
- Validation of finite element predictions with available experimental and numerical results
- Identification of proper ductile fracture criteria
- Implementation of ductile fracture criteria in the computer program for fracture prediction
- Validation of predictions regarding fracture occurrence
- Study the effect of process variables on fracture occurrence

1.4 Organization of the Thesis

The thesis chapters are organized in the following manner:

Chapter 1 discusses the importance of prediction of defects in rolling process. Critical literature review on rolling related to deformation analysis by various methods and ductile fracture is presented. Based on the literature review the scope and objective of the present works is presented. At the end, the way in which the thesis is organized is presented.

Chapter 2 is concerned with the Galerkin finite element formulations to obtain the detailed deformation field in plane-strain cold rolling. A rigid-plastic formulation is presented where the elastic effects are considered to be negligible. In general the generalized stress in the cold rolling material is a function of strain. Therefore, a finite element formulation for the determination of generalized strain distribution is presented. To predict the occurrence of damage by the critical damage criterion of Dhar et al. [1996], distribution of damage variable D over the domain is required. For this distribution of D, a Galerkin finite element formulation is presented which uses the damage law employed by Dhar et al. [1996]. To predict the occurrence of fracture by empirical criterion of Oyane et al. [1980], a Galerkin finite element formulation is presented to determine the distribution of damage variable. At the end, procedure to obtain the secondary variables such as roll torque, roll force and interfacial normal pressure is presented.

In chapter 3, first different fracture criteria used are presented in section 3.2. In section 3.3, predictions of present model are compared with the available experimental and analytical results. Parametric study is carried out to study the influence of process variables on hydrostatic stress distribution, damage distributions of critical damage criterion [Dhar et al., 1996] and Oyane's criterion [Oyane et al., 1980] and the same is presented in sections 3.4.1 to 3.4.3. The effect of process variables on the safe and unsafe zones for fracture is presented in section 3.4.4.

In chapter 4, conclusions and scope for future work is presented.

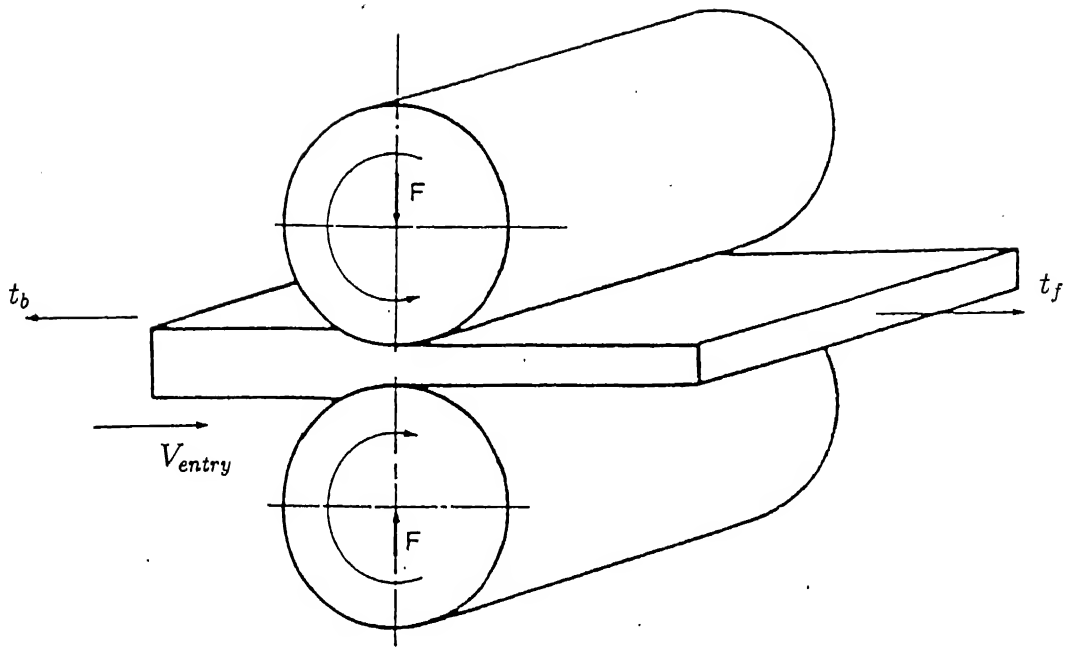

Figure 1.1: Schematic diagram of plane-strain rolling.

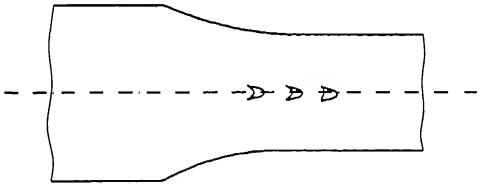

Figure 1.2: Central bursting in plane-strain rolling.

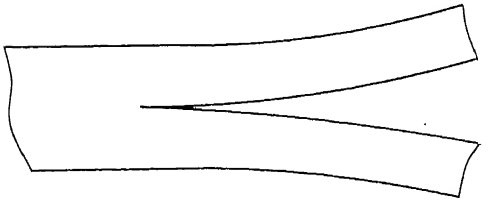

Figure 1.3: Split-end in plane-strain rolling.

Chapter 2

Finite Element Formulation

2.1 Introduction

An important step in the prediction of defects is to develop a fairly exact mathematical model of the process for the determination of the deformation and stress fields. An accurate determination of these fields became possible after the finite element method was developed for the metal forming processes.

In this chapter, Galerkin finite element formulations are presented to obtain the detailed deformation field in steady-state plane-strain rolling process. In section 2.2, a rigid plastic formulation is discussed where the elastic effects are considered to be negligible. In general, the generalized stress of the material is a function of strain for the case of cold rolling. Therefore, one has to know the strain distribution for accurate estimation of the generalized stress. The procedure for determination of strain distribution is presented in section 2.3. To predict the occurrence of fracture by the more realistic criteria, distribution of damage variable over the domain is required. Galerkin finite element formulations are presented in sections 2.4 and 2.5 to determine damage distribution. In section 2.4 damage formulation is for critical damage criterion [Dhar et al., 1996] and in sections 2.5 for Oyane's criterion [Oyane et al., 1980]. The procedure for obtaining the secondary variables is presented at the end of this chapter.

2.2 Rigid-Plastic Formulation

In bulk metal forming processes such as rolling, extrusion, drawing etc., the plastic strains are very large compared to elastic ones. Hence elastic strains can be considered to be insignificant as far as the deformation phenomena are concerned. When the elastic effects

are neglected, then the material behavior is essentially that of a fluid i.e., material incapable of sustaining any deviatoric stress, without motion. Under the assumption of negligible elastic strains, the material can be idealized either as rigid-plastic or rigid-viscoplastic. Deformation of such materials can be conveniently analyzed by Elurian or flow formulation [Zienkiewicz, 1984] and it is with this formulation for plane-strain rolling that this section is concerned.

2.2.1 Constitutive Equation of Rigid-Plastic Material

The system of equations describing the behavior of a solid under various types of response are referred to as the constitutive equations. Steady-state forming processes such as rolling, extrusion, drawing etc., can be conveniently analyzed by using an Eulerian formulation. For such a formulation, the measure of deformation is the strain rate tensor $\dot{\epsilon}_{ij}$, which is expressed as

$$\dot{\epsilon}_{ij} = \frac{1}{2}\left(\frac{\partial V_i}{\partial x_j} + \frac{\partial V_j}{\partial x_i}\right) \tag{2.1}$$

where V_i is the velocity component and x_i represents the coordinate system. In order to express the constitutive equation in a convenient form, the stress tensor σ_{ij} is decomposed as

$$\sigma_{ij} = -p\delta_{ij} + \sigma' ij; \qquad p = -\frac{\sigma_{kk}}{3} \tag{2.2}$$

where p is the (compressive) hydrostatic part, δ_{ij} is the Kronecker's delta and σ'_{ij} is the deviatoric part. Henceforth, the hydrostatic part of σ_{ij} will be denoted by -p and not by σ_m.

The constitutive law for rigid-plastic/ viscoplastic material relating the deviatoric stress tensor σ'_{ij} and the strain rate tensor $\dot{\epsilon}_{ij}$ is expressed as

$$\sigma'_{ij} = 2\mu\dot{\epsilon}_{ij} \tag{2.3}$$

For the material yielding according to von-Mises criterion, the Levy-Mises coefficient μ is given by

$$\mu = \frac{\bar{\sigma}}{3\dot{\bar{\epsilon}}} \tag{2.4}$$

where the generalized stress and strain rate are defined by

$$\bar{\sigma} = \sqrt{\frac{3}{2}\sigma'_{ij}\bar{\sigma}'_{ij}} \tag{2.5}$$

and

$$\dot{\bar{\epsilon}} = \sqrt{\frac{2}{3}\dot{\epsilon}_{ij}\dot{\epsilon}_{ij}} \tag{2.6}$$

In general $\bar{\sigma}$ depends on $\bar{\epsilon}$, $\dot{\bar{\epsilon}}$ and temperature T i.e.,

$$\bar{\sigma} = \mathcal{F}(\bar{\epsilon}, \dot{\bar{\epsilon}}, T) \tag{2.7}$$

Here, the generalized strain $\bar{\epsilon}$ is defined as

$$\bar{\epsilon} = \int_0^t \dot{\bar{\epsilon}} dt \tag{2.8}$$

where the integration is to be carried along the particle path.

2.2.2 Governing Equations

In general, the material behavior of the deforming metal is governed by the equations of conservation of mass, conservation of momentum and conservation of energy. The present formulation deals with the steady-state plane-strain cold rolling where the forming speeds are low and therefore the temperature rise is small. Thus, the process is considered to be isothermal. Therefore, the equation of conservation of energy is not required for the analysis.

In Eulerian reference frame, the momentum equations for a steady-state plane-strain rolling process (neglecting the body forces) have the following form:

$$\rho(V_x \frac{\partial V_x}{\partial x} + V_y \frac{\partial V_x}{\partial y}) = \frac{\partial \sigma'_{xx}}{\partial x} + \frac{\partial \sigma_{xy}}{\partial y} - \frac{\partial p}{\partial x} \tag{2.9}$$

and

$$\rho(V_x \frac{\partial V_y}{\partial x} + V_y \frac{\partial V_y}{\partial y}) = \frac{\partial \sigma_{xy}}{\partial x} + \frac{\partial \sigma'_{yy}}{\partial y} - \frac{\partial p}{\partial y} \tag{2.10}$$

where ρ is the density, V_x and V_y represent the velocity components with respect to the coordinates x, y (Fig. 2.1), p is the hydrostatic part and σ'_{ij} is the deviatoric stress part on the stress tensor σ_{ij}. In plastic deformation, volume remains constant. Therefore, the hydrostatic part of stress is determined from the continuity equation

$$\dot{\epsilon}_{xx} + \dot{\epsilon}_{yy} = 0 \tag{2.11}$$

The relations between strain rate and velocity components for plane-strain problem are given by

$$\dot{\bar{\epsilon}}_{xx} = \frac{\partial V_x}{\partial x} \tag{2.12}$$

$$\dot{\bar{\epsilon}}_{yy} = \frac{\partial V_y}{\partial y} \tag{2.13}$$

$$\dot{\bar{\epsilon}}_{yy} = \frac{1}{2}(\frac{\partial V_x}{\partial y} + \frac{\partial V_y}{\partial x}) \tag{2.14}$$

2.2.3 Boundary Conditions

In the present work, plane-strain strip rolling processes is considered for the analysis. The boundary conditions for the same are discussed in this section.

The boundary conditions specified on any boundary can be classified into three categories. They are *velocity boundary conditions* (specification of velocity components), *stress boundary conditions* (specification of traction components) and *mixed boundary conditions* i.e., combination of one velocity and one stress boundary condition.

The domain along with co-ordinate system for rolling process is shown in Fig. 2.1.

Entry and Exit boundary conditions (AB and EF)

The entry and exit boundaries AB and EF respectively are chosen sufficiently away from the deformation zone so as to take the advantage of uniform conditions prevailing there. Therefore, the conditions on the boundaries AB and EF become

$$V_x = V_{entry}, \qquad V_y = 0 \qquad \text{on } AB \tag{2.15}$$

$$V_x = V_{exit}, \qquad V_y = 0 \qquad \text{on } EF \tag{2.16}$$

where V_{entry} and V_{exit} are respectively the inlet and exit velocity related by

$$V_{entry} = V_{exit}(1 - r) \tag{2.17}$$

where r is the reduction ratio given by $r = \frac{t_o - t_f}{t_o}$.

In a rolling problem inlet and exit velocities are not specified, they can be calculated provided the position of neutral point and roll velocity using the principle of volume constancy.

If front and back tensions are zero, surfaces AB and EF are stress free, then the following boundary conditions can also be applied.

$$V_y = 0; \;\; t_x = 0 \qquad \text{on } \; AB \text{ and } EF \tag{2.18}$$

Free Surfaces (BC and DE)

The boundaries BC and DE are free surfaces, therefore, both t_x and t_y are zero on BC and DE. It is also possible to use the condition $V_y = 0$. In the present work, the following boundary conditions are used:

$$V_y = 0 \text{ and } t_x = 0 \; ion \; AB \text{ and } CD \tag{2.19}$$

The Plane of Symmetry (AF)

The boundary AF is the plane of symmetry, therefore, the following conditions are used:

$$t_x = 0 \text{ and } V_y = 0 \text{ on } AF \tag{2.20}$$

The Roll-Work Interface (CD)

On the roll-work interface, the normal velocity component at any point must be zero. Thus

$$V_n = 0 \Longrightarrow V_y + V_x \tan\phi = 0 \tag{2.21}$$

where ϕ is the angle made by the outward unit normal to the interface at that point with the y-axis.

The second boundary condition is specified in terms of a friction condition. In the present model Coulomb's friction model is used. When Coulomb's law is used, normally a constraint is placed on the maximum value of the shear stress. Thus,

$$|t_s| = f|t_n| \quad \text{when} \quad |t_s| \leq \frac{\bar{\sigma}}{\sqrt{3}} \tag{2.22}$$

and

$$|t_s| = \frac{\bar{\sigma}}{\sqrt{3}} \quad \text{when} \quad |t_s| > \frac{\bar{\sigma}}{\sqrt{3}} \tag{2.23}$$

Here t_s and t_n are the tangential and normal stress components along the interface and f is the coefficient of friction assumed to be constant along the interface.

2.2.4 Galerkin or Weak Formulation

In the present work, mixed pressure-velocity formulation is used. The Galerkin weighted residual method is used to reduce the governing differential equations of the problem into algebraic equations by using appropriate weighted functions for the momentum and continuity equations.

Let V_x, V_y and p be the functions which satisfy all the essential boundary conditions exactly. Then V_x, V_y and p constitute a weak solution if the integral equation,

$$\int_\Omega \left[(\dot{\epsilon}_{xx} + \dot{\epsilon}_{yy}) W_p + \left\{ \rho(V_x \frac{\partial V_x}{\partial x} + V_y \frac{\partial V_x}{\partial y}) + \frac{\partial p}{\partial x} - \frac{\partial \sigma'_{xx}}{\partial x} - \frac{\sigma'_{xy}}{\partial y} \right\} W_x \right.$$

$$\left. + \left\{ \rho(V_x \frac{\partial V_y}{\partial x} + V_y \frac{\partial V_y}{\partial y}) + \frac{\partial p}{\partial y} - \frac{\partial \sigma'_{yy}}{\partial y} - \frac{\sigma'_{xy}}{\partial x} \right\} W_y \right] dx\, dy = 0 \tag{2.24}$$

is satisfied. Here W_p, W_x and W_y are the approximate weight functions which satisfy the homogeneous versions of the boundary conditions and Ω represents the area of the domain.

Performing the integration by parts, on second and third parts of the above equation and using eqn.(2.3), the following weak form is obtained

$$\int_\Omega [I_1 + I_2] \; dx \; dy - \int_{\Gamma_1} I_3 \; d\Gamma_1 - \int_{\Gamma_2} I_4 \; d\Gamma_2 = 0 \tag{2.25}$$

where

$$I_1 = (\dot{\epsilon_{xx}} + \dot{\epsilon_{yy}}) \; W_p \tag{2.26}$$

$$I_2 = \rho\{(V_x \frac{\partial V_x}{\partial x} + V_y \frac{\partial V_x}{\partial y}) \; W_x + (V_x \frac{\partial V_y}{\partial x} + V_y \frac{\partial V_y}{\partial y}) \; W_y$$

$$-p(\dot{\epsilon}_{xx}(W) + \dot{\epsilon}_{yy}(W)) + 2\mu\{\dot{\epsilon}_{xx}\dot{\epsilon}_{xx}(W) + \dot{\epsilon}_{yy}\dot{\epsilon}_{yy}(W) + 2\dot{\epsilon}_{xy}\dot{\epsilon}_{xy}(W)\}\} \tag{2.27}$$

$$I_3 = t_x W_x \tag{2.28}$$

$$I_4 = t_y W_y \tag{2.29}$$

and Γ_1 and Γ_2 are the boundaries where traction components t_x and t_y are specified. The terms $\dot{\epsilon}_{xx}(W)$, $\dot{\epsilon}_{yy}(W)$ and $\dot{\epsilon}_{xy}(W)$ are defined as

$$\dot{\epsilon}_{xx}(W) = \frac{\partial W_x}{\partial x} \tag{2.30}$$

$$\dot{\epsilon}_{yy}(W) = \frac{\partial W_y}{\partial y} \tag{2.31}$$

$$\dot{\epsilon}_{xy}(W) = \frac{1}{2}(\frac{\partial W_x}{\partial y} + \frac{\partial W_y}{\partial x}) \tag{2.32}$$

For finite element formulation, it is convenient to express integral (2.25) in the matrix form as

$$\int_\Omega \left[\{m\}^T\{\dot{\epsilon}\}W_p + \rho\{V_x\{W_x \; W_y\} \begin{Bmatrix} \frac{\partial V_x}{\partial x} \\ \\ \frac{\partial V_y}{\partial x} \end{Bmatrix} + V_y\{W_x \; W_y\} \begin{Bmatrix} \frac{\partial V_x}{\partial y} \\ \\ \frac{\partial V_y}{\partial y} \end{Bmatrix}\} - p\{\dot{\epsilon}(W)\}^T\{m\} \right.$$

$$\left. +2\mu\{\dot{\epsilon}(W)\}^T\{\dot{\epsilon}\} \right] \; dx \, dy - \int_{\Gamma_1} t_x W_x d\Gamma_1 - \int_{\Gamma_2} t_y W_y d\Gamma_2 = 0 \tag{2.33}$$

where

$$\{\dot{\epsilon}\} = \begin{Bmatrix} \dot{\epsilon}_{xx} \\ \dot{\epsilon}_{yy} \\ \sqrt{2}\dot{\epsilon}_{xy} \end{Bmatrix} = \begin{Bmatrix} \frac{\partial V_x}{\partial x} \\ \frac{\partial V_y}{\partial y} \\ \frac{1}{\sqrt{2}}(\frac{\partial V_x}{\partial y} + \frac{\partial V_y}{\partial x}) \end{Bmatrix} \tag{2.34}$$

$$\{\dot{\epsilon}(W)\} = \begin{Bmatrix} \dot{\epsilon}_{xx}(W) \\ \dot{\epsilon}_{yy}(W) \\ \sqrt{2}\dot{\epsilon}_{xy}(W) \end{Bmatrix} = \begin{Bmatrix} \frac{\partial W_x}{\partial x} \\ \frac{\partial W_y}{\partial y} \\ \frac{1}{\sqrt{2}}(\frac{\partial W_x}{\partial y} + \frac{\partial W_y}{\partial x}) \end{Bmatrix} \tag{2.35}$$

and

$$\{m\} = \begin{Bmatrix} 1 \\ 1 \\ 0 \end{Bmatrix} \tag{2.36}$$

2.2.5 Finite Element Approximation

In contrast to the traditional Galerkin weighted residual method where a global approximation is chosen for the field variable, in finite element method the domain of interest is discretized into small elements and the integrals are evaluated over each element after suitably selecting the approximation for the field variable over each element and then the elemental expressions are assembled appropriately to get the global expressions.

From eqn. (2.25), one can see that the convergence and completeness criterion are satisfied if V_x and V_y are chosen to be bilinear and p is chosen to be constant. However, one can use higher order approximation like biquadratic approximation for V_x and V_y and bilinear approximation for p. In the present work, biquadratic approximation for velocities and bilinear approximation for pressure are used (Fig. 2.2). Thus, the approximations for V_x and V_y are

$$\begin{Bmatrix} V_x \\ V_y \end{Bmatrix} = \begin{bmatrix} N_1 & 0 & \cdots & N_9 & 0 \\ 0 & N_1 & \cdots & 0 & N_9 \end{bmatrix} \begin{Bmatrix} (V_x)_1^e \\ (V_y)_1^e \\ \vdots \\ (V_x)_9^e \\ (V_y)_9^e \end{Bmatrix} = [N_v]\{V^e\} \tag{2.37}$$

In Galerkin formulation, the weight functions corresponding to velocities are approximated using the same shape functions as that for velocity. Therefore,

$$\{W_v\} = \begin{Bmatrix} W_x \\ W_y \end{Bmatrix} = [N_v]\{W_v^e\} \tag{2.38}$$

The vectors $\{V^e\}$ and $\{W^e{}_v\}$ contain the nodal values of velocities and the corresponding weight functions, respectively. The approximation for p gives

$$p = \left\{ \begin{array}{cccc} N_1^p & N_2^p & N_3^p & N_4^p \end{array} \right\} \left\{ \begin{array}{c} p_1^e \\ p_2^e \\ p_3^e \\ p_4^e \end{array} \right\} = [N_p]\{p^e\} \tag{2.39}$$

The weight functions corresponding to pressure are approximated using the same shape functions as that for the pressure. Therefore,

$$W_p = [N_p]\{W^e{}_p\} \tag{2.40}$$

The vectors $\{p^e\}$ and $\{W^e{}_p\}$ contains the nodal values of pressure and the corresponding weight functions, respectively. The expressions for the biquadratic (N_i) and bilinear ($N^p{}_i$) shape functions are given in any standard text book [Reddy, 1993] which deals with the finite element method.

In the present work, the geometry is also approximated by the same shape functions as that used for velocities. Therefore,

$$x = [N]\{x^e\}; \quad y = [N]\{y^e\} \tag{2.41}$$

The vectors $\{x^e\}$ and $\{y^e\}$ contain the nodal values of x and y coordinates respectively and $\{N\}$ is the one-dimensional array of quadratic shape functions as

$$\{N\} = \left\{ \begin{array}{cccc} N_1 & N_2 & \cdots & N_9 \end{array} \right\} \tag{2.42}$$

To evaluate the integrals over boundaries Γ_i, an approximation for the weight functions over these boundaries is needed. The approximation consistent with the interior approximations (eqn. 2.38) is

$$W_x = \left[\begin{array}{ccc} N_1^b & N_2^b & N_3^b \end{array} \right] \left\{ \begin{array}{c} W_{vx}^1 \\ W_{vx}^2 \\ W_{vx}^3 \end{array} \right\} = \{N_b\}\{W_x^b\} \tag{2.43}$$

and

$$W_y = \left[\begin{array}{ccc} N_1^b & N_2^b & N_3^b \end{array} \right] \left\{ \begin{array}{c} W_{vy}^1 \\ W_{vy}^2 \\ W_{vy}^3 \end{array} \right\} = \{N_b\}\{W_y^b\} \tag{2.44}$$

where N_i^b are the one-dimensional Lagrangian quadratic shape functions and $\{W_x^b\}$ and $\{W_y^b\}$ are the vectors of the nodal values of the weight functions for a typical boundary element shown in Fig. 2.3. Further t_x and t_y are approximated as

$$t_x = \left[\begin{array}{ccc} N_1^b & N_2^b & N_3^b \end{array} \right] \left\{ \begin{array}{c} t_{bx}^1 \\ t_{bx}^2 \\ t_{bx}^3 \end{array} \right\} = \{N_b\}\{t_x^b\} \tag{2.45}$$

and

$$t_y = \left[\begin{array}{ccc} N_1^b & N_2^b & N_3^b \end{array} \right] \left\{ \begin{array}{c} t_{by}^1 \\ t_{by}^2 \\ t_{by}^3 \end{array} \right\} = \{N_b\}\{t_y^b\} \tag{2.46}$$

where $\{t_x^b\}$ and $\{t_y^b\}$ are the vectors of the nodal values of the traction.

2.2.6 Finite Element Equations

Using the approximations (2.37) and (2.38), the strain rate components and the corresponding derivatives of the weight functions can be expressed in the vector forms as given below.

The strain rate vector $\{\dot{\epsilon}\}$ and the vector $\{\dot{\epsilon}(W)\}$ become

$$\{\dot{\epsilon}\} = [B]\{V^e\} \tag{2.47}$$

and

$$\{\dot{\epsilon}(W)\} = [B]\{W_v^e\} \tag{2.48}$$

where

$$[B] = \left[\begin{array}{cccccc} \frac{\partial N_1}{\partial x} & 0 & \cdots & \frac{\partial N_9}{\partial x} & 0 \\ 0 & \frac{\partial N_1}{\partial y} & \cdots & 0 & \frac{\partial N_9}{\partial y} \\ \frac{1}{\sqrt{2}}\frac{\partial N_1}{\partial y} & \frac{1}{\sqrt{2}}\frac{\partial N_1}{\partial x} & \cdots & \frac{1}{\sqrt{2}}\frac{\partial N_9}{\partial y} & \frac{1}{\sqrt{2}}\frac{\partial N_9}{\partial x} \end{array} \right] \tag{2.49}$$

By substituting the above vector expressions along with the boundary approximations (eqn. 2.43 to 2.46) the integral (eqn. 2.33) becomes

$$\Sigma_{e=1}^{NEM}\{W^e\}^T[K^e]\{X^e\} = \Sigma_{b=1}^{NBEX}\{W_x^b\}^T\{f_x^b\} + \Sigma_{b=1}^{NBEY}\{W_y^b\}^T\{f_y^b\} \tag{2.50}$$

where

$$\{W^e\} = \left\{ \begin{array}{c} \{W_p^{(e)}\} \\ \{W_v^{(e)}\} \end{array} \right\} \tag{2.51}$$

$$\{X^e\} = \left\{ \begin{array}{c} \{p^{(e)}\} \\ \{V^{(e)}\} \end{array} \right\} \tag{2.52}$$

$$\{K^e\} = \left[\begin{array}{cc} [0] & [K_{pv}^e] \\ [K_{vp}^e] & [K_{vv}^e] \end{array} \right] \tag{2.53}$$

$$[K_{pv}^e] = -\int_{A^e} [N_p]^T\{m\}^T[B]\, dx\, dy \tag{2.54}$$

$$[K^e_{vp}] = -\int_{A^e} [B]^T\{m\}[N_p]\, dx\, dy \tag{2.55}$$

$$[K^e_{vv}] = \int_{A^e} 2\mu[B]^T[B]\, dx\, dy + \int_{A^e} \rho\left(V_x[N_v]^T\frac{\partial N_v}{\partial x} + V_y[N_v]^T\frac{\partial N_v}{\partial y}\right) dx\, dy \tag{2.56}$$

$$\{f^b_x\} = \int_{\Gamma^b_1} \{N_b\}^T\{N_b\}[t^b_x]\, d\Gamma \tag{2.57}$$

$$\{f^b_y\} = \int_{\Gamma^b_2} \{N_b\}^T\{N_b\}[t^b_y]\, d\Gamma \tag{2.58}$$

Here, NEM is the number of area elements, NBEX is the number of boundary elements on Γ_1 and NEBY is the number of boundary elements on Γ_2. A^e denotes the domain of a typical area element while Γ^b_1 and Γ^b_2 are the domains of typical boundary elements on Γ_1 and Γ_2, respectively.

For the purpose of numerical evaluation, the variables of the area integrals (2.54to2.56) are transformed to the natural coordinates (ζ, η) using the following transformation:

$$\int_{A^e}(...)\, dx\, dy = \int_{-1}^{+1}\int_{-1}^{+1}(...)|J|\, d\zeta\, d\eta \tag{2.59}$$

where $|J|$ is the determinant of the elemental Jacobian matrix and is given by

$$|J| = \begin{bmatrix} \frac{\partial x}{\partial \zeta} & \frac{\partial x}{\partial \eta} \\ \\ \frac{\partial y}{\partial \zeta} & \frac{\partial y}{\partial \eta} \end{bmatrix} \tag{2.60}$$

Here, the co-ordinates (x,y) are approximated using the biquadratic shape functions.

Similarly the boundary integrals are transformed to integrals over the interval (-1,1) by the relation

$$\int_{\Gamma}(...)d\Gamma = \int_{-1}^{+1}(...)|J_b|d\zeta \tag{2.61}$$

where $|J_b|$ is the Jacobian for the boundary element and is given by

$$|J_b| = \sqrt{\left(\frac{\partial x}{\partial \zeta}\right)^2 + \left(\frac{\partial u}{\partial \zeta}\right)^2} \tag{2.62}$$

Along the boundary, the co-ordinates (x, y) are approximated using 1-D quadratic shape functions. All the elemental matrices are evaluated using the 3X3 Gauss quadrature. Similarly the elemental vectors (2.57 and 2.58) are evaluated using 3 point Gauss quadrature.

The assembly of elemental coefficient matrices into the global coefficient matrix is done by transforming the elements corresponding to a local degree of freedom to positions of

corresponding global degrees of freedom in the global coefficient matrix. Similar procedure is followed for the assembly of global boundary matrix. The assembled finite element equation can be written as

$$\{W\}^T[K]\{X\} = \{W\}^T\{F\} \tag{2.63}$$

where $\{W\}$ is the global vector of nodal values of weight functions, $[K]$ is the global coefficient matrix, $\{X\}$ is the global vector of nodal values of pressure and velocities and $\{F\}$ is the global right side vector. Since $\{W\}$ is arbitrary, the final expression is given by

$$[K]\{X\} = \{F\} \tag{2.64}$$

The above equation has to be solved after substitution of the boundary conditions. The procedure for the application of boundary conditions is discussed in the next section.

2.2.7 Application of Boundary Conditions

The natural boundary conditions on the tool-work interface can be applied without evaluating the boundary matrices $\{f_x^b\}$ and $\{f_y^b\}$ in the manner described below.

The Coulomb friction condition (2.23)at a typical node on the tool work interface (Fig. 2.3) is given by

$$|t_s| = f|t_n| \tag{2.65}$$

After expressing t_s and t_n in terms of t_x and t_y at that node and rearranging the terms, the above equation becomes

$$t_x(\cos\phi - f\ k_s\ \sin\phi) - t_y(\sin\phi + f\ k_s\ \cos\phi) = 0 \tag{2.66}$$

where k_s is -1 before neutral point and +1 after neutral point. In the present work, ϕ is assumed to be constant over a boundary element and equal to the angle at the middle node of the element because it does not change much over a element. Then the above expression for an element can be written as

$$\left\{ \begin{array}{c} t_{bx}^1 \\ t_{bx}^2 \\ t_{bx}^3 \end{array} \right\} (1 - f\,k_s\,\tan\phi) - \left\{ \begin{array}{c} t_{by}^1 \\ t_{by}^2 \\ t_{by}^3 \end{array} \right\} (\tan\phi + f\,k_s) = 0 \tag{2.67}$$

After multiplying above equation by

$$\int_{-1}^{+1} \{N_b\}^T\{N_b\}|J_b|d\zeta \tag{2.68}$$

it becomes

$$\{f_x^b\}(1 - f\ k_s \tan\phi) - \{f_y^b\}(\tan\phi + f\ k_s) = \{0\} \tag{2.69}$$

The above equation holds good at all the nodes of the element. At the middle node say 'k' (global node number), there is no contribution from the neighboring elements and therefore, in terms of global right side vector, above equation can be written as

$$\{F\}_{(d_p+2k-1)}(1 - f\ k_s \tan\phi) - \{F\}_{(d_p+2k)}(\tan\phi + f\ k_s) = 0 \tag{2.70}$$

where d_p is the total number of pressure variables. At the end node also, the above eqn. (2.70) holds good provided contribution of the adjacent element is added to it. Thus, the procedure for applying the condition (2.65) at a boundary node 'k' is as follows:

- Replace $(d_p + 2k - 1)th$ row of global coefficient matrix [K] by the following condition:

$(1-fk_s \tan\phi)$ times $(d_p + 2k - 1)th$ row of $[K]-(\tan\phi+fk_s)$ times $(d_p + 2k)th$ row of $[K]$.

- Make the $(d_p + 2k - 1)^{th}$ row of global right hand vector {F} as zero.

The velocity boundary condition at the node is applied replacing $(d_p + 2k)th$ row of [K] by the eqn. (1.22).

- Make $(d_p + 2k)th$ row of [K] zero.
- Set $(d_p + 2k, d_p + 2k - 1)th$ element of [K] to $\tan\phi$ and $(d_p + 2k, d_p + 2k)th$ element of [K] to 1.
- Make $(d_p + 2k)th$ row of {F} to zero.

2.2.8 Estimation of Neutral Point

In order to apply the natural boundary condition on the roll-strip interface, the location of the neutral point has to be known. In this formulation, the neutral point is found by minimizing total power with respect to the position of the neutral point.

A generalized upper bound theorem [Collins, 1969] is expressed by,

$$\int_{S_u} t_i v_i^* ds \leq \int_V \sigma_{ij}^* \dot{\epsilon}_{ij}^* dV - \int_{S_F} t_i v_i^* ds \tag{2.71}$$

where S_F is the part of surface where some or all of the traction components are specified and S_u is the remainder of the surface. Here, S_u is the boundary CD while S_F includes all other boundaries. It is assumed that on parts AB and EF, instead of the velocity

component v_x, it is the stress component t_x which is specified with values equal to back (t_b) and front (t_f) tensions respectively. Further, v_i^* is any piece-wise continuous velocity field defined over volume V with corresponding strain-rate field $\dot{\epsilon}_{ij}^*$, and σ_{ij}^* is the plastic stress field related to $\dot{\epsilon}_{ij}^*$ through the flow rule. Here v_i^* is a volume preserving velocity field, but does not have to be a kinematically admissible field. But in our formulation, v_i^* is so chosen that v_n^* is satisfies all the velocity boundary conditions also. Further, v_s^* can be expressed as the sum of roll velocity (V_R) and relative sliding velocity of strip ($v_s^* - V_R$). Therefore, the above inequality becomes,

$$\int_{BC} t_s V_R ds \leq \int_V \sigma_{ij}^* \dot{\epsilon}_{ij}^* dV + \int_{AF} t_b v_x^* ds - \int_{DE} t_f v_x^* ds + \int_{BC} t_s (v_s^* - V_R) ds. \qquad (2.72)$$

where v_n^* and v_s^* are the normal and tangential components of v_i^* on interface. The integral on the left side of the inequality is the actual rolling power and the integrals on the right side are plastic power, power due to tensions and friction power respectively, being based on the assumed velocity field. The computations of plastic power and power due to tensions pose no problem, whilest for the computation of friction power (last integral of the inequality), actual shear traction distribution is required which in not known beforehand. Avitzur [1964] has assumed its magnitude to be $f(\sigma_y)_0/\sqrt{3}$, where f is a friction factor. In the present model, t_s is obtained from eqn. (2.23) in which t_n is obtained from the solution of continuity and momentum equations, at assumed location of neutral point. This t_n is found to be approximately close to the actual t_n except near assumed neutral point. However, since the relative velocity between the roll and strip is very small near the assumed neutral point, the error in the evaluation of friction power is negligible. Thus, all the three components of power are computed for different assumed positions of neutral point and the position which minimizes the sum of these is treated as the correct position of neutral point [Dixit and Dixit 1996].

2.2.9 Solution Procedure

After imposing the boundary conditions as discussed in the above section, the final matrix is solved iteratively by Householder method [Bathe, 1990]. The Householder method is used because the resulting matrix of the mixed formulation is ill-conditioned. For the first iteration, the value of μ is obtained from the upper bound velocity field. For the inlet and outlet regions a suitable guess is used. This value is updated by using the velocity field of previous iteration. For each assumed position of neutral point, the iterations are continued until the nodal velocity and pressure values converge within 0.1% between the successive iterations for finding out corresponding power. The position of neutral point

corresponding to the minimum power is considered as the correct one. In the process of numerical simulation, the value of μ becomes very large outside the deformation zone as the generalized strain rate is near to zero in those regions. This high value of μ makes the coefficient matrix more ill-conditioned. This difficulty is overcome by prescribing a suitable cut off value for μ.

2.3 Formulation for Strain Hardening

To updated the value of μ, in the rigid-plastic formulation, the generalized stress stress $\bar{\sigma}$ need to be updated. In general $\bar{\sigma}$ is a function of $\bar{\epsilon}$ for the metals which are cold rolled. Therefore, the procedure to obtain the distribution of $\bar{\epsilon}$ over the domain is presented in this section.

The generalized strain $\bar{\epsilon}$ is obtained by integrating the generalized strain rate $\dot{\bar{\epsilon}}$ along path line (eqn. 2.6) and is given by

$$\bar{\epsilon} = \int_0^t \dot{\bar{\epsilon}} dt \tag{2.73}$$

Alternately, one can convert the above equation into a differential equation [Avitzur and Talbert, 1989] as

$$\frac{d\bar{\epsilon}}{dt} = \dot{\bar{\epsilon}} \tag{2.74}$$

where $\frac{d\bar{\epsilon}}{dt}$ is the material time derivative. For plane-strain steady-state problem, the above equation can be written as

$$V_x \frac{\partial \bar{\epsilon}}{\partial x} + V_y \frac{\partial \bar{\epsilon}}{\partial y} = \dot{\bar{\epsilon}} \tag{2.75}$$

Since the deformation at the beginning of the inlet zone negligible, the initial condition for this differential equation is

$$\bar{\epsilon} = 0 \ \text{ on } \ AB \tag{2.76}$$

Galerkin formulation of eqn. (2.75) over an element gives the following integral:

$$\Sigma_{e=1}^{NEM} \int_{A^e} (V_x \frac{\partial \bar{\epsilon}}{\partial x} + V_y \frac{\partial \bar{\epsilon}}{\partial y} - \dot{\bar{\epsilon}}) W_{\bar{\epsilon}} \, dx \, dy = 0 \tag{2.77}$$

where $W_{\bar{\epsilon}}$ is the weighting function. The above equation can be written in matrix form as

$$\Sigma_{e=1}^{NEM} \int_{A^e} \left[\{V_x \ \ V_y\} \begin{Bmatrix} \frac{\partial \bar{\epsilon}}{\partial x} \\ \\ \frac{\partial \bar{\epsilon}}{\partial y} \end{Bmatrix} - \dot{\bar{\epsilon}} \right] W_{\bar{\epsilon}} \, dx \, dy = 0 \tag{2.78}$$

In the present work, the generalized strain and the corresponding weight function are approximated by the same shape functions as used for the velocity approximation. Therefore,

$$\bar{\epsilon} = \{N\}\{\bar{\epsilon}^e\} \tag{2.79}$$

$$W_{\bar{\epsilon}} = \{N\}\{W_{\bar{\epsilon}}^e\} \tag{2.80}$$

Here vectors $\{\bar{\epsilon}^e\}$ and $\{W_{\bar{\epsilon}}^e\}$ contain the elemental nodal values of $\bar{\epsilon}$ and $W_{\bar{\epsilon}}$. The vector containing the derivatives in eqn. (2.78) above can be written as

$$\left\{ \begin{array}{c} \frac{\partial \bar{\epsilon}}{\partial x} \\ \\ \frac{\partial \bar{\epsilon}}{\partial y} \end{array} \right\} = [H]\{\bar{\epsilon}^e\} \tag{2.81}$$

where

$$[H] = \left[\begin{array}{cccc} \frac{\partial N_1}{\partial x} & \frac{\partial N_2}{\partial x} & \cdots & \frac{\partial N_9}{\partial x} \\ \\ \frac{\partial N_1}{\partial y} & \frac{\partial N_2}{\partial y} & \cdots & \frac{\partial N_9}{\partial y} \end{array} \right] \tag{2.82}$$

After substituting the approximations for generalized strain, the weighting function, the vector containing the strain derivatives and velocity vector, the final expression can be written as

$$\Sigma_{e=1}^{NEM}\{W_{\bar{\epsilon}}^e\}^T[K_{\bar{\epsilon}}^e]\{\bar{\epsilon}^e\} = \Sigma_{e=1}^{NEM}\{W_{\bar{\epsilon}}^e\}^T\{f_{\bar{\epsilon}}^e\} \tag{2.83}$$

where

$$[K_{\bar{\epsilon}}^e] = \int_\Omega ([N]^T\{V^e\}^T[N_v]^T[H])\, dx\, dy \tag{2.84}$$

$$\{f_{\bar{\epsilon}}^e\} = \int_\Omega (\{N\}^T\dot{\bar{\epsilon}})\, dx\, dy \tag{2.85}$$

Here, $[K_{\bar{\epsilon}}^e]$ and $\{f_{\bar{\epsilon}}^e\}$ are the elemental coefficient matrix and the right hand side vector respectively for the evaluation of generalized strain. Since $\{W_{\bar{\epsilon}}^e\}^T$ is arbitrary, the final global matrices can be written as

$$[K_{\bar{\epsilon}}]\{\bar{\epsilon}\} = \{F_{\bar{\epsilon}}\} \tag{2.86}$$

where $[K_{\bar{\epsilon}}]$ is the global coefficient matrix, $\{\bar{\epsilon}\}$ is the global vector of the nodal values of $\bar{\epsilon}$ and $\{F_{\bar{\epsilon}}\}$ is the global right side vector.

The generalized strain distribution obtained by solving the above equation is used to update the value of generalized stress $\bar{\sigma}$. This $\bar{\sigma}$ is used to update the value of μ present in the matrices of the rigid-plastic finite element formulations.

2.4 Damage Formulation

2.4.1 Formulation for Critical Damage Criterion [Dhar et al., 1996]

In the present work, one of the criteria used for prediction of central burst is the critical value of the damage variable. For evaluation of the damage, the continuum damage mechanics model employed by Dhar et al. [1996] is used. The model has been described in section 1.2. of chapter 1. For the sake of completeness, some salient features of the model have been reproduced below.

Damage represents surface discontinuities in the form of micro-crack or volume discontinuities in the form of micro-voids. They assumed that the discontinuities are spread in an isotropic way. Then the damage variable is considered as a scalar. In the model proposed by Dhar et al. [1996], D is defined as the area void fraction at a point.

The material behavior of a damaged material is influenced by the damage i.e., the constitutive equation of such a material depends on the damage variable. For some materials like high carbon steel, the damage level at failure are quite low, of the order of 0.05 [Dhar et al., 1996]. Therefore, for such materials the damage variable does not affect significantly either the deformation field or the stress field. As a result, for such materials, it is possible to decouple the damage evaluation law from the constitutive relation. In that case, one can first determine the deformation and stress fields using the constitutive relation of the undamaged material and then evaluate the damage with the help of damage evaluation law.

Dhar et al. [1996] proposed a damage evaluation law based on the damage growth model of Lemaitre [1985] and the experimental results of Ley Roy et al. [1981] and is given by

$$\frac{dD}{dt} = C_D\dot{\bar{\epsilon}} + (a_1 + a_2 D)(-Y)\dot{\bar{\epsilon}} \tag{2.87}$$

where -Y, the variable conjugate to D, is given by

$$-Y = \frac{\bar{\sigma}^2}{2E} f(\frac{\sigma_m}{\bar{\sigma}}) \tag{2.88}$$

$$f(\frac{\sigma_m}{\bar{\sigma}}) = \frac{2(1+\nu)}{3} + 3(1-2\nu)(\frac{\sigma_m}{\bar{\sigma}})^2 \tag{2.89}$$

The model incorporates the damage growth due to both the void nucleation as well as the void growth.

For plane-strain problem, the above equation can be written as

$$V_x \frac{\partial D}{\partial x} + V_y \frac{\partial D}{\partial y} - C_D \dot{\bar{\epsilon}} - (a_1 + a_2 D)(-Y)\dot{\bar{\epsilon}} = 0 \tag{2.90}$$

Since the damage growth at the beginning of the inlet zone is insignificant, the initial condition for this differential equation is

$$D = 0 \qquad \text{on } AB \quad \text{(Fig. 2.1)} \tag{2.91}$$

Galerkin formulation of the eqn. (2.90) over an element gives the following integral:

$$\Sigma_{e=1}^{NEM} \int_{A^e} \left\{ V_x \frac{\partial D}{\partial x} + V_y \frac{\partial D}{\partial y} - C_D \dot{\bar{\epsilon}} - (a_1 + a_2 D)(-Y)\dot{\bar{\epsilon}} \right\} W_D \, dx \, dy = 0 \tag{2.92}$$

where W_D is weighting function. The above integral can be written in the matrix form as

$$\Sigma_{e=1}^{NEM} \int_{A^e} \left[\{V_x \quad V_y\} \begin{Bmatrix} \frac{\partial D}{\partial x} \\ \\ \frac{\partial D}{\partial y} \end{Bmatrix} - a_2 D(-Y)\dot{\bar{\epsilon}} - (C_D + a_1(-Y))\dot{\bar{\epsilon}} \right] W_D \, dx \, dy = 0 \tag{2.93}$$

In the present work, the damage variable D and the corresponding weight function W_D are approximated by the same shape functions as used for the velocity approximation. Therefore,

$$D = \{N\}\{D^e\} \tag{2.94}$$

$$W_D = \{N\}\{W_D^e\} \tag{2.95}$$

Here $\{D^e\}$ and $\{W_D^e\}$ contain the nodal values of D and W_D. The vector containing the derivatives of D can be written as

$$\begin{Bmatrix} \frac{\partial D}{\partial x} \\ \\ \frac{\partial D}{\partial y} \end{Bmatrix} = [H]\{D^e\} \tag{2.96}$$

where [H] has already been defined in eqn. (2.82). After substituting the approximations for D, W_D, the vector containing the derivatives of D and the velocity vector, the final expression can be written as

$$\Sigma_{e=1}^{NEM} \{W_D^e\}^T [K_D^e] \{D^e\} = \Sigma_{e=1}^{NEM} \{W_D^e\}^T \{f_D^e\} \tag{2.97}$$

where

$$[K_D^e] = \int_{A^e} \left[[N]^T \{V^e\}^T [N_v]^T [H] - a_2(-Y)\{N\}^T \{N\}\dot{\bar{\epsilon}} \right] dx \, dy \tag{2.98}$$

$$\{f_D^e\} = \int_{A^e} \{N\}^T (C_D + a_1(-Y))\dot{\bar{\epsilon}} \, dx \, dy \tag{2.99}$$

Here $[K_D^e]$ and $\{f_D^e\}$ are the elemental coefficient matrix and right side vector respectively for the evaluation of damage D. Since $\{W_D^e\}^T$ is arbitrary, the final global matrices can be written as

$$[K_D]\{D\} = \{F_D\} \tag{2.100}$$

where $[K_D]$ is the global coefficient matrix, $\{D\}$ is the global vector of the nodal values of D and $\{F_D\}$ is the global right side vector.

While solving the above equation, Y is calculated from the deviatoric stress field and the pressure field of the rigid-plastic solution of eqn. (2.64).

2.4.2 Formulation for Oyane's Criterion [Oyane et al., 1980]

In this section, Galerkin finite element formulation for Oyane's fracture criterion is presented for prediction of defects in rolling, which is proposed by Oyane et al. [1980]. The model has been described in section 1.2. of chapter 1.

Oyane et al. [1980] used the plasticity theory for porous materials to propose a ductile fracture criterion indicating that micro crack initiates whenever the volumetric strain reaches a material dependent critical value C. They proposed a empirical criterion which is given by

$$\int_0^{\bar{\epsilon}_f} (1 + \frac{\sigma_m}{A\bar{\sigma}})\, d\bar{\epsilon} = C \tag{2.101}$$

where $\bar{\epsilon}_f$ is the generalized strain at which fracture occurs, C and A are material constants. This integral can also be written as

$$\frac{dC}{d\bar{\epsilon}} = (1 + \frac{\sigma_m}{A\bar{\sigma}}) \tag{2.102}$$

and also,

$$\frac{dC}{dt} = (1 + \frac{\sigma_m}{A\bar{\sigma}})\dot{\bar{\epsilon}} \tag{2.103}$$

For plane-strain problem, the above equation can be written as

$$V_x \frac{dC}{dx} + V_y \frac{dC}{dy} = (1 + \frac{\sigma_m}{A\bar{\sigma}})\dot{\bar{\epsilon}} \tag{2.104}$$

Since the Damage growth at the beginning of the inlet zone is insignificant, the initial condition for differential equation is

$$C = 0 \text{ on } AB \tag{2.105}$$

Galerkin formulation of the eqn.(2.104) over an element gives the following integral:

$$\Sigma_{e=1}^{NEM} \int_{A^e} \left\{ V_x \frac{\partial C}{\partial x} + V_y \frac{\partial C}{\partial y} - (1 + \frac{\sigma_m}{A\bar{\sigma}})\dot{\bar{\epsilon}} \right\} W_C \, dx \, dy = 0 \tag{2.106}$$

where W_C is weighting function. the above integral can be written in the matrix form as

$$\Sigma_{e=1}^{NEM} \int_{A^e} \left[\{V_x \quad V_y\} \begin{Bmatrix} \frac{\partial C}{\partial x} \\ \\ \frac{\partial C}{\partial y} \end{Bmatrix} - (1 + \frac{\sigma_m}{A\bar{\sigma}})\dot{\bar{\epsilon}} \right] W_C \, dx \, dy = 0 \tag{2.107}$$

In the present work, the damage variable C and the corresponding weight function W_C are approximated by the same shape functions as used for the velocity approximation. Therefore,

$$C = \{N\}\{C^e\} \tag{2.108}$$

$$W_C = \{N\}\{W_C^e\} \tag{2.109}$$

Here $\{C^e\}$ and $\{W_C^e\}$ contain the nodal values of C and W_C. The vector containing the derivatives of C can be written as

$$\begin{Bmatrix} \frac{\partial C}{\partial x} \\ \\ \frac{\partial C}{\partial y} \end{Bmatrix} = [H]\{C^e\} \tag{2.110}$$

where [H] has already been defined in eqn. (2.82). After substituting the approximations for C and W_C, the vector containing the derivatives of C and the velocity vector, the final expression can be written as

$$\Sigma_{e=1}^{NEM} \{W_C^e\}^T [K_C^e] \{C^e\} = \Sigma_{e=1}^{NEM} \{W_C^e\}^T \{f_C^e\} \tag{2.111}$$

where

$$[K_C^e] = \int_{A^e} \left[[N]^T \{V^e\}^T [N_v]^T [H] \right] \, dx \, dy \tag{2.112}$$

$$\{f_C^e\} = \int_{A^e} (1 + \frac{\sigma_m}{A\bar{\sigma}})\dot{\bar{\epsilon}} \, dx \, dy \tag{2.113}$$

Here $[K_C^e]$ and $\{f_C^e\}$ are the elemental coefficient matrix and right side vector respectively for the evaluation of damage C. Since $\{W_C^e\}^T$ is arbitrary, the final global matrices can be written as

$$[K_C]\{C\} = \{F_C\} \tag{2.114}$$

where $[K_C]$ is the global coefficient matrix, $\{C\}$ is the global vector of the nodal values of C and $\{F_C\}$ is the global right side vector.

In order to apply the Oyane's criterion, the availability of the material dependent constant A and C is necessary. With this aim Alberti et al. [1993] have been carried out some upsetting tests on cylindrical specimens of aluminium alloy (UNI 3571). They obtained values of A and C, they are 0.24 and 0.348 respectively.

2.5 Secondary Quantities

From the above formulations one can obtain the primary variables only, namely the nodal velocities, pressure, deviatoric stresses etc. The procedure for obtaining the secondary quantities from them is described in this section.

Roll Torque (T)

The roll torque is calculated from the relationship

$$T = \frac{PR}{V_R} \tag{2.115}$$

where the total power P consists of the following three parts,

Power required for plastic deformation (P_p)

The power dissipated due to plastic deformation is given by

$$P_p = \int_A \sigma_{ij}\dot{\epsilon}_{ij}\, dx\, dy \tag{2.116}$$

Power required to overcome friction at the roll-strip interface (P_f)

The power dissipated due to friction is given by

$$P_f = \int_0^l |t_s||\Delta V_s| ds \tag{2.117}$$

where ΔV_s is the relative velocity with respect to the velocity of neutral point along the interface and l is the arc of contact. The shear stress t_s is calculated from eqn. (2.23).

Power due to tensions (P_t)

The power required in the presence of front and back tensions is

$$P_t = (t_b - t_f)\frac{h_0}{2}\, V_{entry} \tag{2.118}$$

Roll pressure of interfacial normal stress (t_n)

At a typical boundary node shown in Fig.(3), the normal pressure can be expressed as

$$t_n = t_x\, n_x + t_y\, n_y \tag{2.119}$$

where $n_y = \cos\phi$ and $n_x = \sin\phi$. now by using expression $t_i = \sigma_{ij} n_j$ the above equation can be written as

$$t_n = \sigma_{xx} {n_x}^2 + \sigma_{yy} {n_y}^2 + 2\sigma_{xy} n_x n_y \tag{2.120}$$

To get the stress value at the interface, first the stresses are calculated at 3X3 Gauss points in the element and then extrapolated to 3 points on the interface.

Roll force (F_r)

The roll force is the component of the resultant of interfacial stresses which is given by

$$F_r = \int_0^{\mathbf{l}} (t_n \cos\phi - t_s \sin\phi)\, ds. \tag{2.121}$$

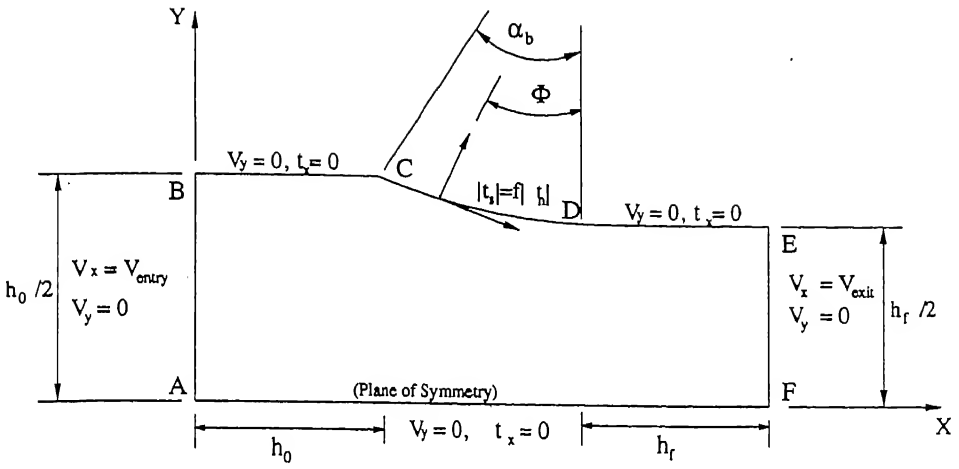

Figure 2.1: The Domain and the boundary conditions (velocity and traction) for plane-strain rolling.

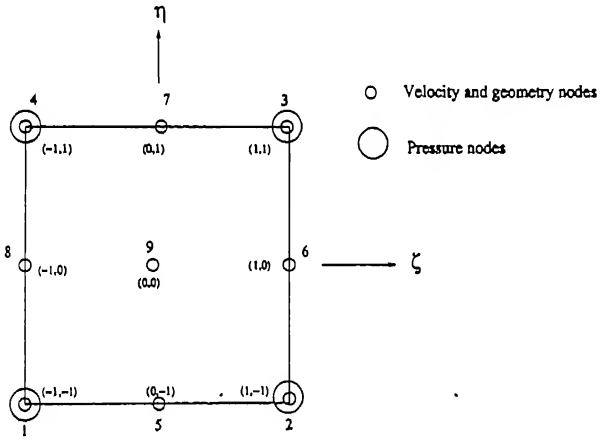

Figure 2.2: Typical area element.

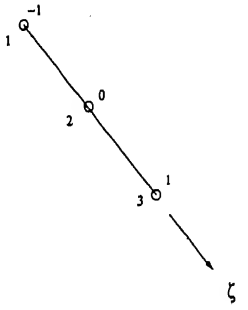

Figure 2.3: Typical boundary element.

Chapter 3

Results and Discussions

3.1 Introduction

The finite element model presented in chapter 2 is implemented using Fortran language and applied to analyze plane-strain rolling process. The results are obtained using three metals. The metals considered being aluminium, copper and steel. These metals are chosen, so the comparison with experimental work is facilitated.

In section 3.2, fracture criteria namely hydrostatic stress criterion [Reddy et al., 1996], critical damage criterion [Dhar et al., 1996] and Oyane's criterion [Oyane et al., 1980] are presented.

To test the predictions (pressure, force and torque) of the present model, its predictions are compared with the experimental results of Al-Salehi et al. [1973] and Shida and Awazuhara [1973] and also with the finite element results of Dixit [1997] and are presented in sections 3.3.1 and 3.3.2. In section 3.3.3, the predictions of HSC are compared with the available experimental results of Turckzyn and Malinowski [1996] for alligatoring.

Comprehensive parametric study is carried out to study the influence of process variables on the hydrostatic stress and damage distributions [Dhar et al., 1996; Oyane et al., 1980] and are presented in sections 3.4.1 to 3.4.3. Parametric study for studying the effect of process variables on the boundary between safe and unsafe zone for fracture is carried out using fracture criteria namely hydrostatic stress criterion [Reddy et al., 1996] and critical damage criterion [Dhar et al., 1996] and the same is presented in section 3.4.4.

3.2 Fracture Criterion

Different fracture criteria used to predict the fracture initiation are presented in this section. Three criteria namely hydrostatic stress criterion [Reddy et al., 1996], critical damage criterion [Dhar et al., 1996] and Oyane's criterion [Oyane et al., 1980] are used to predict the central burst and only HSC is used to predict the split-ends in rolling.

3.2.1 Hydrostatic Stress Criterion (HSC) [Reddy et al., 1996]

If the process conditions are such that hydrostatic stress is tensile in the deformation zone, then micro-voids first get nucleated, then they grow and finally coalesce with one another leading to micro-crack initiation. If one can maintain the compressive hydrostatic stress in the deformation zone, then the micro-voids either do not nucleate or the existing micro-voids remain closed and, thus, there is no possibility of micro-crack initiation. The work of Clift et al. [1990] shows that the value of hydrostatic stress at fracture initiation in extrusion is close to zero. Based on these observations Reddy et al. [1996] proposed the hydrostatic stress criterion to predict the central burst in extrusion, and the same is used in the present work to predict the central burst in rolling.

Criterion for Central burst

Whenever hydrostatic stress at a point on the centerline in the deformation zone becomes zero and is compressive elsewhere, there is fracture initiation leading to central burst.

Criterion for Alligatoring

When the damage is severe it leads to alligatoring or split-end defect. Alligatoring also nucleates as a micro-void, leading to micro-crack, forming along the central plane of the deformed material (the plane connecting the axis of symmetry of the rolls). As the rolling proceeds two "halves" of the material separates from each other and alligatoring occurs. It will occur when the tensile hydrostatic stress at the axis of symmetry reaches the order of yield stress of the material. Based of this hydrostatic stress criterion to predict split-end is proposed as:

"Whenever the tensile hydrostatic stress value at a point on the centerline in the deformation zone reaches the order of yield stress, the split-end defect will occur".

3.2.2 Critical Damage Criterion [Dhar et al., 1996]

Dhar et al. [1995] reported that for SAE 1090 steel, micro-crack initiation arises whenever the value of damage variable D reaches the critical value (D_c) of 0.05. The same is used in present work to predict the central burst initiation in rolling.

3.2.3 Oyane's Criterion [Oyane et al., 1980]

Alberti et al. [1993] reported that for aluminium alloy (UNI 3571), fracture occurs whenever the value of damage variable C in Oyane's criterion [Oyane et al. 1980] reaches the critical value (C_c) of 0.348.

3.3 Validation

3.3.1 Comparison of Pressure Predictions

Pressure predictions of the present model are compared with the experimental results of Al-Salehi et al. [1973]. Figures (3.1) and (3.2) shows the variation of roll pressure with the angle of contact for copper and aluminium respectively. It can be seen that the predicted results are in reasonable agreement with the experimental results of Al-Salehi et al. [1973]. The general shapes of the experimental and predicted distributions are similar, there being differences in magnitude. The difference in magnitude can be attributed to the roll deformation which is neglected in the present work.

Pressure predictions of the present model are compared with the finite element results of Dixit [1997] (Figures (3.1) and (3.2)). It can be seen from the figures (3.1) and (3.2) that predictions of both the models are in good agreement. However shift in neutral point towards the exit has been observed in case of aluminium. The discrepancy between the two results can be attributed to roll deformation and variation of friction coefficient, which is considered by Dixit [1997].

3.3.2 Comparison of Force and Torque Predictions

Force and torque predictions of the present model are compared with the experimental results of Al-Salehi et al. [1973] for aluminium and copper and Shida and Awazuhara [1973] for steel. Figures (3.3) to (3.5) shows the variation of roll separating force with the reduction in area for aluminium, copper and steel respectively. Figures (3.6) to (3.8) shows the variation of roll torque with the reduction for aluminium, copper and steel respectively.

It can be seen from the figures 3.3 to 3.8, at the lower reductions the discrepancy between the predicted and experimental results is low. At higher reductions the discrepancy between experimental and predicted results is high. This can be attributed to increase in roll deformation with reduction. In case of aluminium (Figures 3.3 and 3.6) and copper (Figures 3.4 and 3.7) the discrepancy at higher reductions also very less compared to steel (Figures 3.5 and 3.8), this is mainly due to the roll deformation which will be higher in case of steel. In the present model roll deformation is not considered.

Roll force and torque predicted in the present model are also compared with the finite element predictions of Dixit [1997] (Figures (3.3) to (3.8)). There is a good agreement between predicted and finite element results of Dixit [1997]. However there is a discrepancy in magnitude this can be attributed to the roll deformation and variation in friction which is not considered in the present work.

3.3.3 Validation of HSC

Reddy et al. [1996] proposed hydrostatic stress criterion to predict central burst in extrusion. They compared the prediction of HSC with the available experimental results and showed that there is a good agreement between HSC predictions and experimental results. The same HSC is used in the present work to predict central burst in rolling. Critical literature survey carried out to find the experimental results to compare the prediction of HSC for central burst but, the attempt was unsuccessful.

To establish the validity of the HSC predictions for split-ends/ alligatoring of the present work, these results are compared with the available experimental results of Turckzyn and Malinowski [1996]. They carried out experiments using an aluminium alloy (6061-T6) of rectangular bars of 6.35, 7.94, 9.35 and 12.7 mm of height with 25.4 mm of width. They used two pairs of rolls having radii 21 and 67 mm, to obtain results at eight values (0.095, 0.118, 0.139, 0.189, 0.302, 0.378, 0.44 and 0.605) of parameter (h_0/R_0). These experimental condition may not be satisfying plane-strain deformation conditions but, they compared these results with their plane-strain upper bound results. The material properties for annealed aluminium alloy as give by Turckzyn and Malinowski [1995] are

$$\text{Generalized stress } (\bar{\sigma}) = 24.83[1 + 57.74\,\bar{\epsilon}]^{\,0.204} \text{ MPa} \quad (3.1)$$

$$\text{Generalized stress at zero plastic strain } (\sigma_0) = 43 \text{ MPa} \quad (3.2)$$

Avitzur et al. [1988] also used the same parameter (h_0/R_0) to obtain the safe and unsafe zone boundary for central burst as well as split-ends. Hence, from these works [Avitzur et

al., 1988, Turckzyn and Malinowski, 1996], it can be concluded that safe and unsafe zone for defect is independent of (h_0) and (R_0), and depends on the parameter (h_0/R_0).

Turckzyn and Malinowski [1996] used roll of 67 mm radius, to obtain results at first four values of parameter (h_0/R_0) (0.095, 0.118, 0.139 and 0.189). It can be seen from the Fig. 3.9 that they carried out experiments in the range of 0.03 to 0.16 reductions. Except few stray points, defect is not occurred in this range. For remaining four values of parameter (h_0/R_0) (0.302, 0.378, 0.44 and 0.605) using roll radius of 21 mm, they carried out experiments in the range of 0.05 to 0.27 reductions. Fig. 3.9 shows that the defect occurred upto 0.16, 0.18 and 0.24 reductions at h_0/R_0 values of 0.302, 0.378 and 0.44 respectively.

In the present work, to establish the validity of the hydrostatic stress criterion, its predictions for split-ends are compared with experimental results of Turckzyn and Malinowski [1996]. It is assumed that alligatoring occurs whenever the ratio of hydrostatic stress to material yield stress ratio (σ_m/σ_0) is within the limits of -0.85 and -1.15. Occurrence of split-ends is predicted at values of h_0/R_0 from 0.095, 0.118, 0.139, 0.189, 0.302, 0.378 and 0.44 at the same conditions as used by Turckzyn and Malinowski [1996]. In the present work friction coefficient is taken as 0.1. To predict the split-end occurrence at values of h_0/R_0 from 0.095 to 0.189, using roll radius 67 mm, executions are carried out. It is observed that from reduction 0.03 to 0.17 there is no occurrence of defect. Using roll radius 21 mm executions are carried out at three values (0.302, 0.378 and 0.44) of parameter h_0/R_0 and defects are not predicted above the reductions 0.19, 0.25 and 0.29 respectively. Although, the thickness to width ratio used for carrying out experiments by Turckzyn and Malinowski [1996] is not in the plane-strain range, they are compared with the predictions of the present work which assumes the deformation to be plane strain. From the above observations, it can be seen that the predictions of the present work using HSC for split-ends are in good agreement with the experimental results of Turckzyn and Malinowski [1996].

It is observed that keeping (h_0/R_0) parameter value constant, if the values of h_0 and R_0 are changed, the hydrostatic stress distribution remains same but the value of compressive hydrostatic stress is varying. This can be seen from Figures 3.10 (a) and (b). Hence, the boundary between safe and unsafe zone is not independent of h_0 and R_0 and also not dependent on (h_0/R_0).

3.4 Parametric Study

Parametric study is carried out to study the influence of process variables (reduction in area, friction and roll radius) on the hydrostatic stress distribution, damage distribution of critical damage criterion [Dhar et al., 1996] and damage distribution of Oyane's criterion [Oyane et al., 1980]. Parametric study for studying the effect of process variables on the safe and unsafe zone for fracture is carried out using fracture criteria (hydrostatic stress criterion [Reddy et al., 1996] and critical damage criterion [Dhar et al., 1996]) and the same is presented in section 3.4.4.

3.4.1 Hydrostatic Stress Distribution

The results in this section are obtained by choosing SAE 1090 steel, the material properties for SAE 1090 steel as given by Le Roy et al. [1981] are

$$\text{Generalized stress } (\bar{\sigma}) = 1115\ (\bar{\epsilon})^{0.19}\ \text{MPa} \quad (3.3)$$

$$\text{Generalized stress at zero plastic strain } (\sigma_0) = 464\ \text{MPa} \quad (3.4)$$

$$\text{Modulus of Elasticity (E)} = 210\ \text{GPa} \quad (3.5)$$

$$\text{Poisons ratio } (\nu) = 0.3 \quad (3.6)$$

Hydrostatic stress plays a major role in ductile fracture. Therefore, for prediction of ductile fracture, it is necessary to know the effect of process variables on the hydrostatic stress distribution. Figure 3.11 shows the hydrostatic stress distribution for a typical set of process conditions (Material: SAE 1090 steel, % r = 10, f = 0.075, R = 65 mm). It is observed that the hydrostatic stress is compressive everywhere in the deformation zone, but becomes tensile at the boundary in a small region near the exit of the roll-work interface. Figure 3.12 shows that the hydrostatic stress distribution remains same with increase in reduction in area but the value of compressive hydrostatic stress is increasing with increase in reduction. When the friction is decreased (Fig. 3.13), the distribution remains same with an increase in compressive stress value in the deformation zone. With increase in roll radius (Fig. 3.14) the compressive hydrostatic stress is decreasing. This can be attributed to increase in homogeneity of deformation with roll radius.

3.4.2 Damage Distribution [Dhar et al., 1996]

The results in this section are obtained by choosing SAE 1090 steel as the work piece material. This material is chosen because of the availability of data that are required for applying the fracture criterion of Dhar et al. [1996]. The material properties of SAE 1090 steel are given in above section.

Figure 3.15 shows the damage distribution for a set of process parameters (Material: SAE 1090 steel, % r = 10, f = 0.075, R = 65 mm). It is observed that value of the damage variable is increasing along the plane of symmetry and reaching maximum at exit of the roll-work interface. Fig. 3.16 shows that there is no change in damage distribution with increase in reduction but the value of damage increasing in the deformation zone. This can be attributed to the increase in inhomogeneity of the deformation with increase in reduction. Fig. 3.17 shows that there is no significant change in damage distribution with decrease in friction coefficient. However, the maximum value of damage variable is slightly decreasing with decrease in friction coefficient. Fig. 3.18 shows the variation of damage distribution with roll radius. With the increase in roll radius the max value of damage in the deformation zone is decreased, this is mainly due to increase in homogeneity of deformation with roll radius. In all these (Figures 3.15 to 3.18) damage distribution contours damage variable is multiplied by 10.

3.4.3 Damage Distribution [Oyane et al., 1980]

The results of this section are obtained by choosing aluminium alloy (UNI 3571) as the workpiece material. This material is chosen because of the availability of data that are required for applying the Oyane's criterion [Oyane et al., 1980]. Properties of this alloy given by [Alberti et al., 1993]

$$\text{Generalized stress } (\bar{\sigma}) = 574\,(\bar{\epsilon})^{\,0.141}\ \text{MPa} \tag{3.7}$$

$$\text{Generalized stress at zero plastic strain } (\sigma_0) = 300\ \text{MPa} \tag{3.8}$$

Figure 3.19 shows the damage distribution for a typical set of process parameters (% r = 10, f = 0.075, R = 65 mm). It is observed that value of the damage variable is increasing along the plane of symmetry and reaching maximum at exit of the roll-work interface. It is observed that with the increase in reduction the maximum damage value also increasing along the plane of symmetry (Fig. 3.20). This can be attributed to the increase inhomogeneity of deformation. The maximum value of damage value is decreasing with decrease in friction (Fig 3.21), this can be attributed to the decrease in inhomogeneity

of deformation. With increase in roll radius the maximum value of the damage is decreasing (Fig 3.22). This can be attributed to the increase in deformation length with roll radius there by decrease in inhomogeneity of deformation.

3.4.4 Safe and Unsafe Zones for Defects

3.4.4.1 Hydrostatic Stress Criterion

Predictions of this section are obtained by using SAE 1090 steel, the properties of this material are given in section (3.2.3).

Alligatoring

Fig. 3.23 shows the boundary between safe and unsafe zone for perfectly-plastic and strain hardening material. It can be observed that for strain hardening material the safe zone is less compared to perfectly plastic material. This trend is similar to that of Turckzyn and Malinowski [1996]. Fig. 3.24 shows the variation of safe and unsafe zone with respect to variation in coefficient of friction. As the coefficient of friction increases the boundary between safe and unsafe zone is moving towards higher reduction, i.e., reduction in safe zone. This can be attributed to decrease in hydrostatic stress with increase in friction. Where as the zone is moving towards less reduction with increase in roll radius (Fig. 3.25), this can be attributed to the increase in deformation length with increase in roll radius there by increase in homogeneity of deformation. A typical hydrostatic stress distribution at split-end condition is shown in Fig. 3.26.

Central Burst

Figures 3.27 and 3.28 shows the change in boundary between safe and unsafe zone with change in roll radius and coefficient of friction respectively. It can be observed that safe zone is increased with decrease in friction or increase in roll radius. These effects are similar to that of alligatoring observed in above section. Fig. and 3.29 shows the typical hydrostatic stress at central bursting condition.

3.4.4.2 Critical Damage Criterion [Dhar et al., 1996]

Predictions of this section are obtained by using SAE 1090 steel, the properties of this material are given in section 3.4.2.

Figures 3.30 and 3.31 shows the changes in safe and unsafe zone boundaries with change in roll radius and friction coefficient respectively. Figures 3.30 shows that with increase in roll radius the boundary between safe and unsafe zone is moving towards lower reductions. Figures 3.31 shows that with friction coefficient the boundary between safe and unsafe zone is moving towards higher reduction. These predictions shows the similar trend as the HSC predictions shown in above section. A typical damage distribution at fracture conditions is shown in Fig. 3.32. In Fig. 3.32 damage variable is multiplied by 10.

It can be observed that predictions of HSC for central burst is always above the critical damage criterion. Hence it can be said HSC is more conservative as mentioned by Reddy et al. [1996].

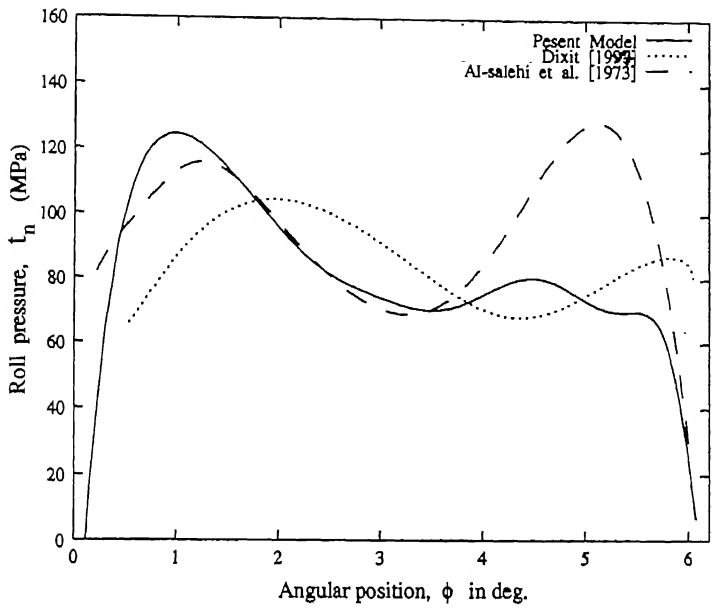

Figure 3.1: Comparison with experimental and finite element results for roll pressure [Material: aluminium, $\bar{\sigma} = 50.3\ (1 + \bar{\epsilon}/0.050)^{\ 0.26}$ MPa, R = 79.375 mm, $h_0 = 6.274$ mm, f = 0.1, % r = 14.17]

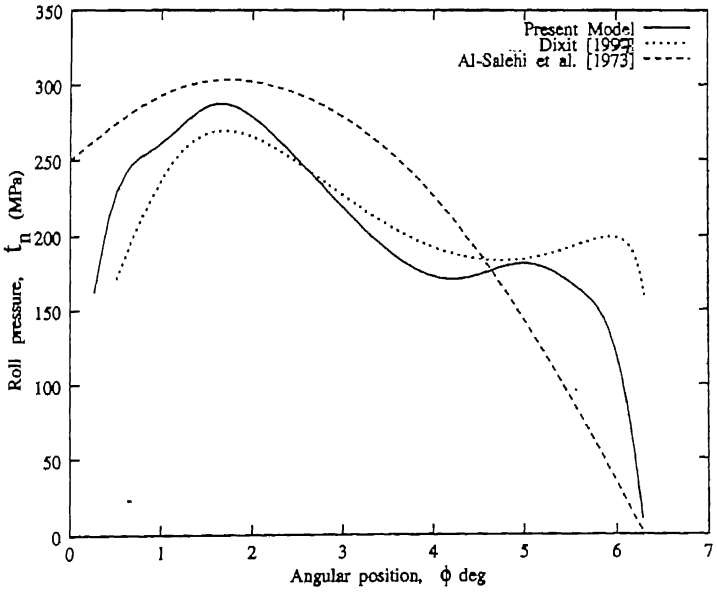

Figure 3.2: Comparison with experimental and finite element results for roll pressure [Material: copper, $\bar{\sigma} = 70.3\ (1 + \bar{\epsilon}/0.022)^{\ 0.49}$ MPa, R = 79.375 mm, $h_0 = 6.35$ mm, f = 0.06, % r = 14.80]

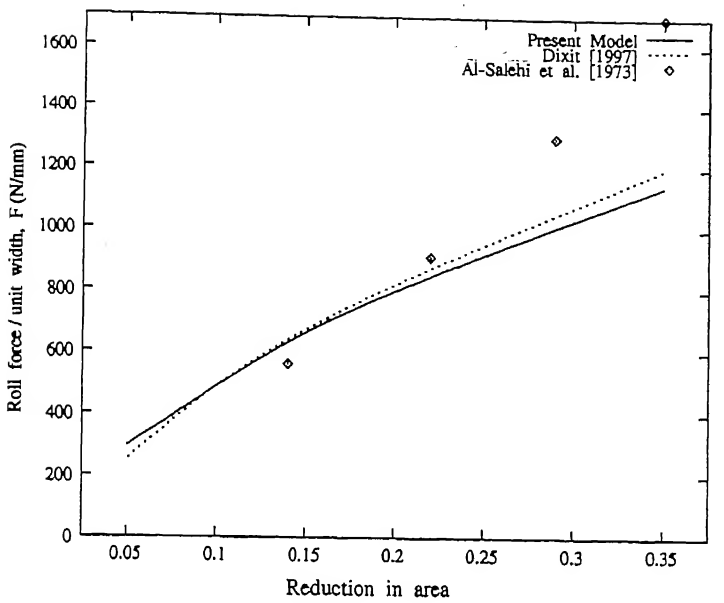

Figure 3.3: Roll force comparison with finite element and experimental results [Material: aluminium, $\bar{\sigma} = 50.3\ (1 + \bar{\epsilon}/0.050)^{\ 0.26}$ MPa, $h_0 = 6.274$ mm, R = 79.375 mm, f = 0.10]

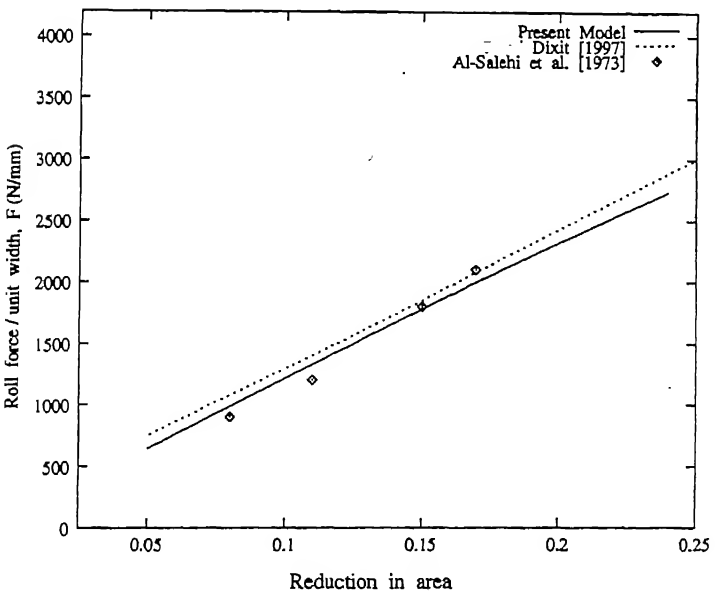

Figure 3.4: Roll force comparison with finite element and experimental results [Material: copper, $\bar{\sigma} = 70.3\ (1 + \bar{\epsilon}/0.022)^{\ 0.49}$ MPa, $h_0 = 6.35$ mm, R = 79.375 mm, f = 0.06]

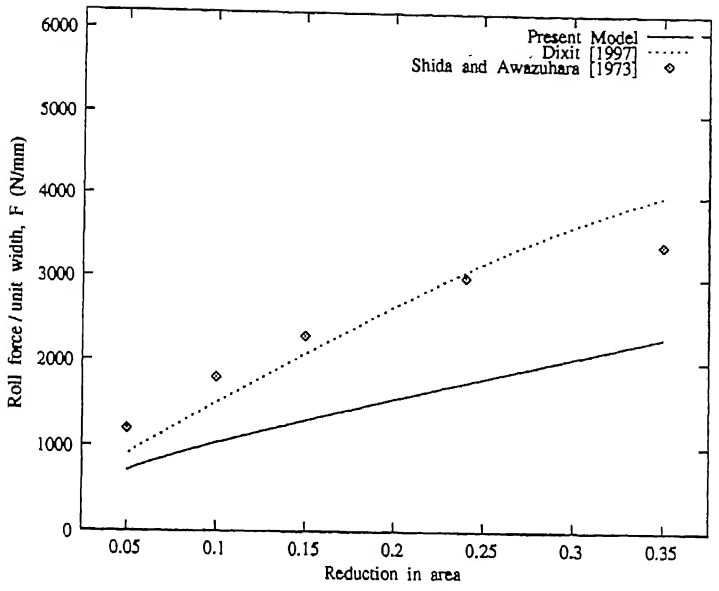

Figure 3.5: Roll force comparison with finite element and experimental results [Material: steel, $\bar{\sigma} = 324.0\ (1 + \bar{\epsilon}/0.052)^{\ 0.295}$ MPa, $h_0 = 1$ mm, R = 65 mm, f = 0.08]

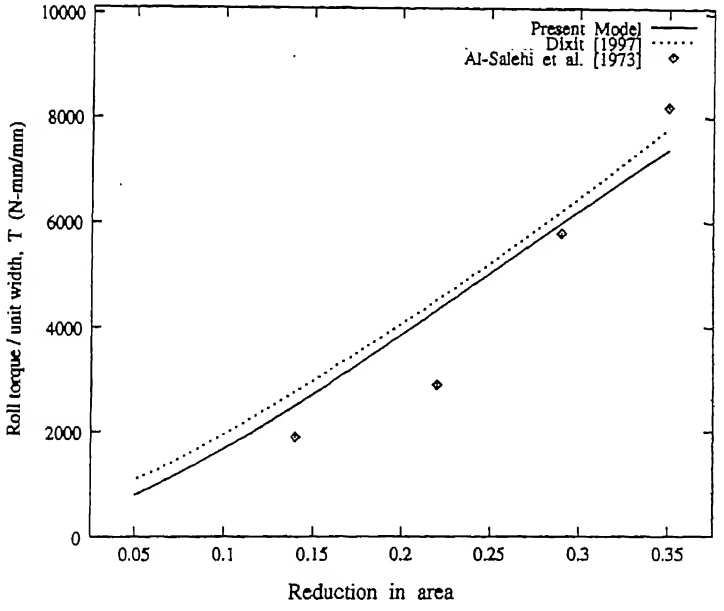

Figure 3.6: Roll torque comparison with finite element and experimental results [Material: aluminium, $\bar{\sigma} = 50.3\ (1 + \bar{\epsilon}/0.050)^{\ 0.26}$ MPa, $h_0 = 6.274$ mm, R = 79.375 mm, f = 0.10]

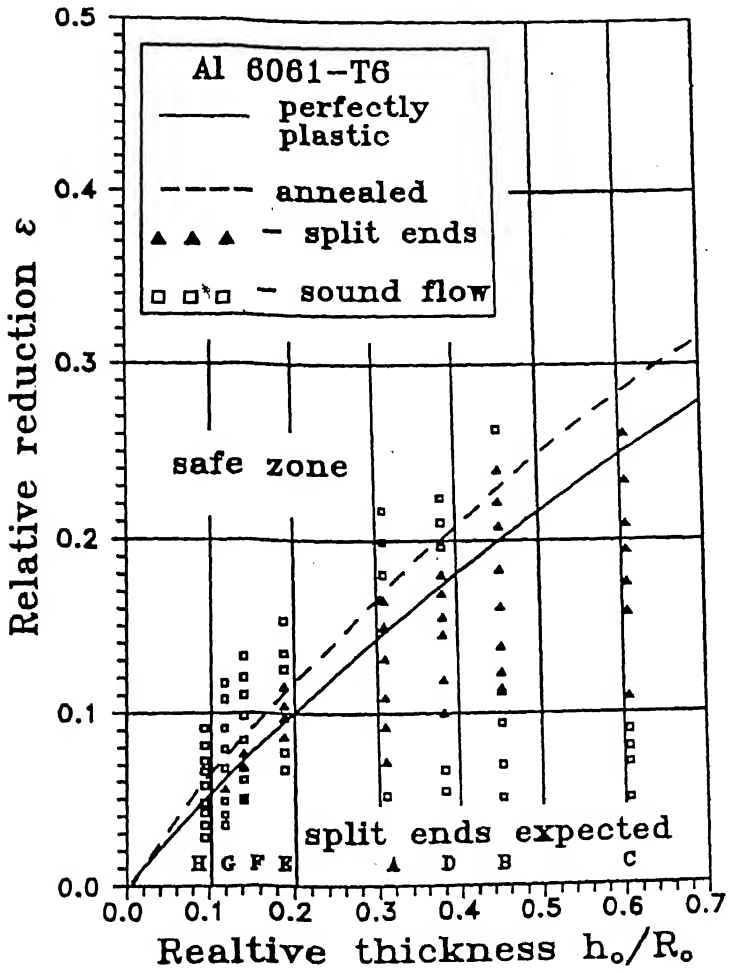

Figure 3.9: Analytical and experimental results of Turckzyn and Malinowski [1996] for split-ends

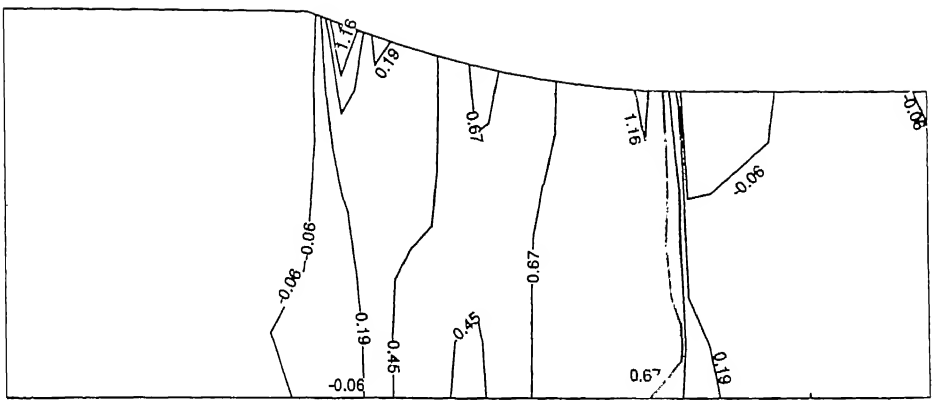

(a)

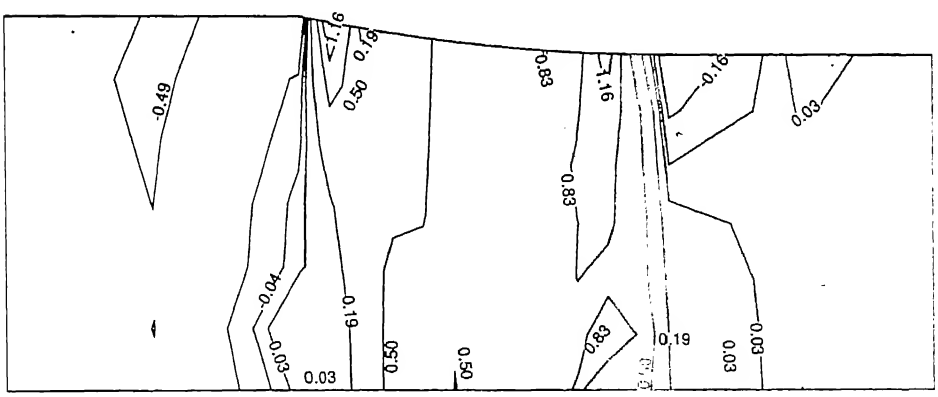

(b)

Figure 3.10: Hydrostatic stress ($\frac{p}{\sigma_0}$) distribution at $(h_0/R_0) = 0.1$ (a) $h_0 = 1$ mm, $R_0 = 65$ mm, (b) $h_0 = 2$ mm, $R_0 = 130$ mm [Material: SAE 1090 steel, $\bar{\sigma} = 1115\ \bar{\epsilon}^{0.19}$ MPa, f = 0.08]

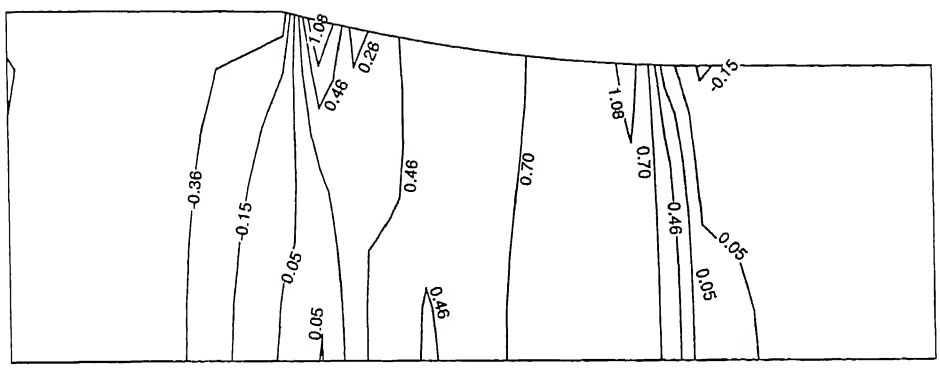

Figure 3.11: Hydrostatic stress $(\frac{p}{\sigma_0})$ distribution [Material: SAE 1090 steel, $\bar{\sigma} = 1115\ \bar{\epsilon}^{0.19}$ MPa, % r = 10, f = 0.075, R = 65 mm]

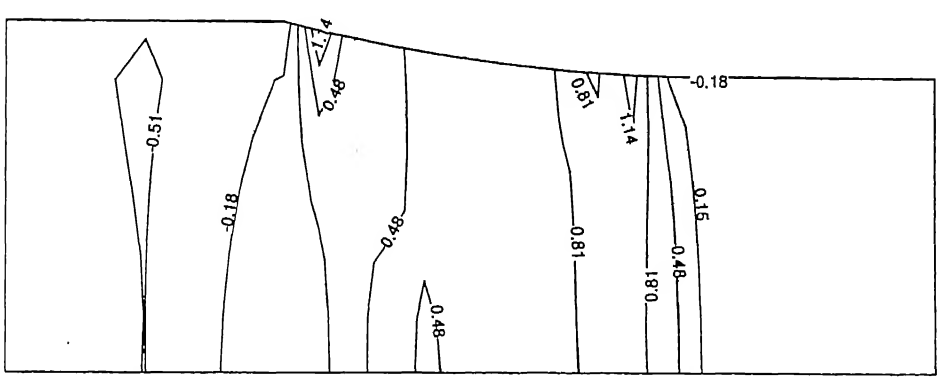

Figure 3.12: Hydrostatic stress $(\frac{p}{\sigma_0})$ distribution [Material: SAE 1090 steel, $\bar{\sigma} = 1115\ \bar{\epsilon}^{0.19}$ MPa, % r = 15, f = 0.075, R = 65 mm]

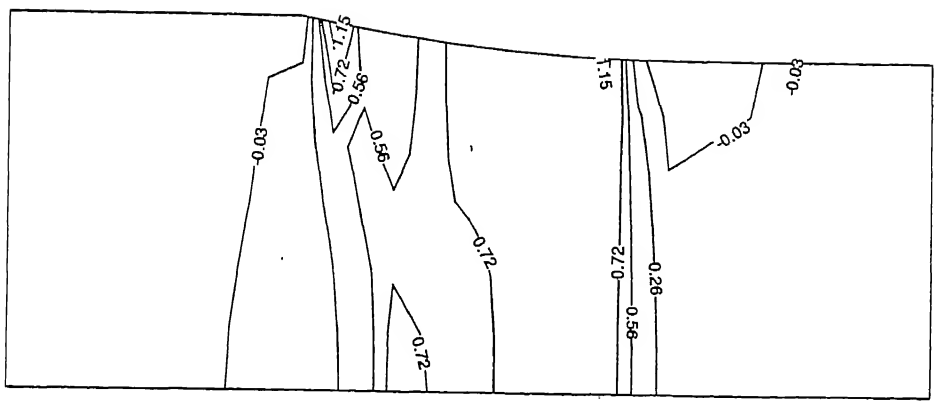

Figure 3.13: Hydrostatic stress $(\frac{p}{\sigma_0})$ distribution [Material: SAE 1090 steel, $\bar{\sigma} = 1115\ \bar{\epsilon}^{0.19}$ MPa, % r = 10, f = 0.05, R = 65 mm]

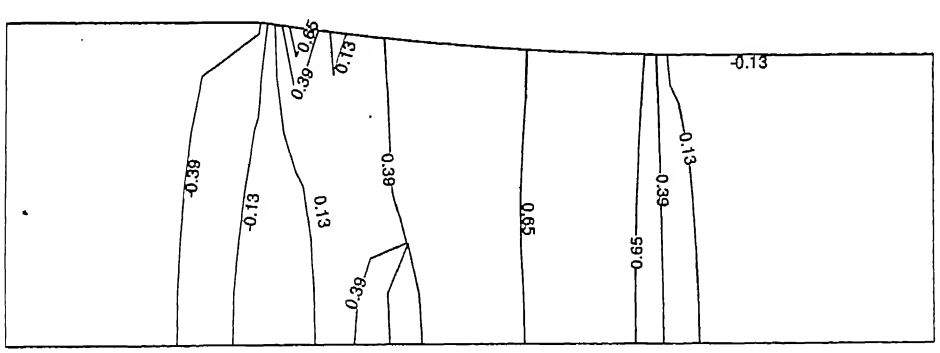

Figure 3.14: Hydrostatic stress $(\frac{p}{\sigma_0})$ distribution [Material: SAE 1090 steel, $\bar{\sigma} = 1115\ \bar{\epsilon}^{0.19}$ MPa, % r = 10, f = 0.075, R = 130 mm]

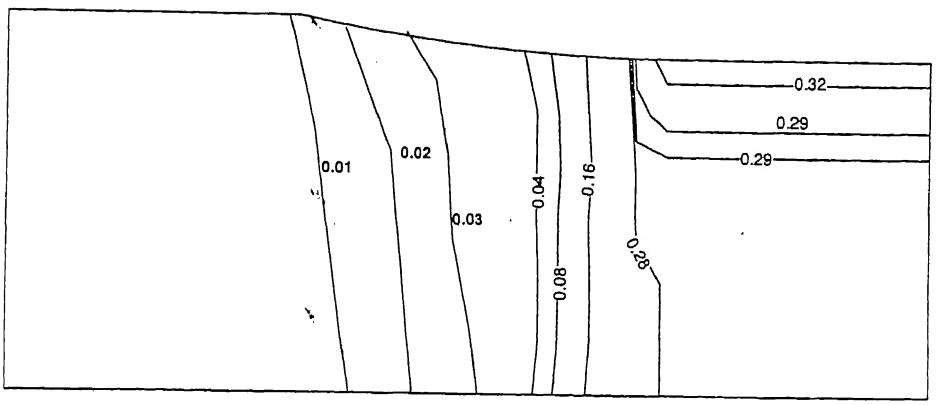

Figure 3.15: Damage distribution in plane-strain rolling, critical damage criterion [Dhar et al., 1996] (DX10) [Material: SAE 1090 steel, $\bar{\sigma} = 1115\ \bar{\epsilon}^{\,0.19}$ MPa, % r = 10, f = 0.075, R = 65 mm]

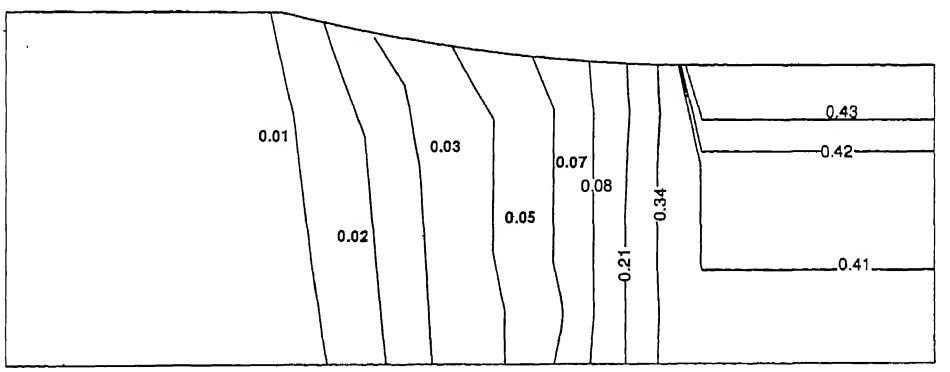

Figure 3.16: Damage distribution in plane-strain rolling, critical damage criterion [Dhar et al., 1996] (DX10) [Material: SAE 1090 steel, $\bar{\sigma} = 1115\ \bar{\epsilon}^{\,0.19}$ MPa, % r = 15, f = 0.075, R = 65 mm]

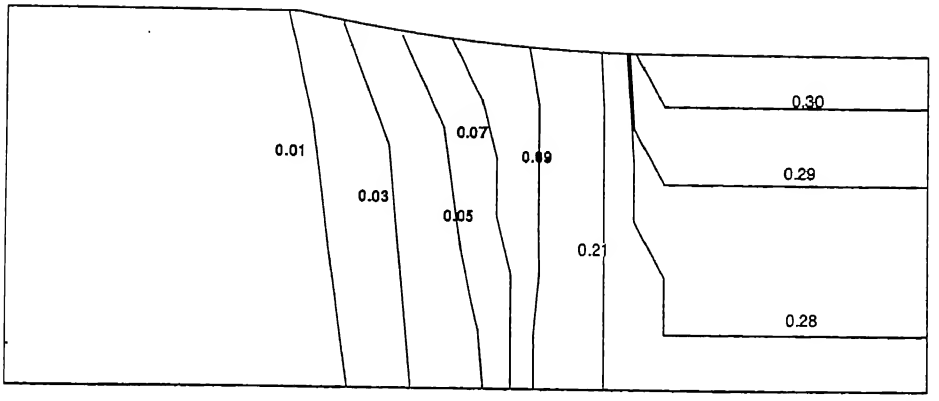

Figure 3.17: Damage distribution in plane-strain rolling, critical damage criterion [Dhar et al., 1996] (DX10) [Material: SAE 1090 steel, $\bar{\sigma} = 1115\ \bar{\epsilon}^{\,0.19}$ MPa, % r = 10, f = 0.05, R = 65 mm]

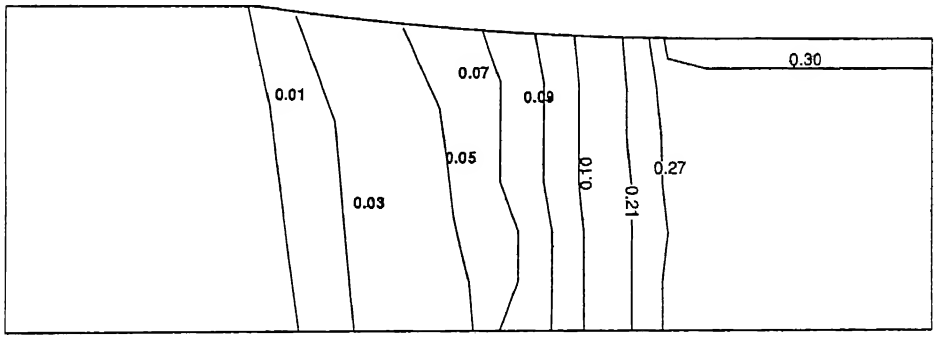

Figure 3.18: Damage distribution in plane-strain rolling, critical damage criterion [Dhar et al., 1996] (DX10) [Material: SAE 1090 steel, $\bar{\sigma} = 1115\ \bar{\epsilon}^{\,0.19}$ MPa, % r = 10, f = 0.075, R = 130 mm]

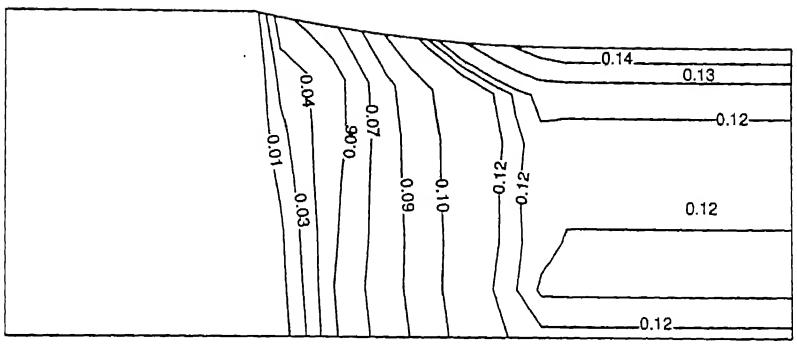

Figure 3.19: Damage distribution in plane strain rolling, Oyane's criterion [Oyane et al., 1980] (Material: aluminium alloy (UNI 3571), $\bar{\sigma} = 574\ \bar{\epsilon}^{0.141}$ MPa, % r = 10, f = 0.075, R = 65 mm)

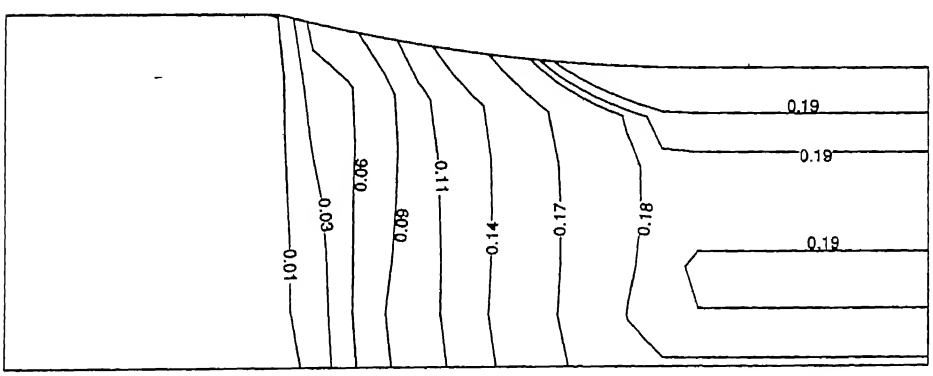

Figure 3.20: Damage distribution in plane strain rolling, Oyane's criterion [Oyane et al., 1980] (Material: aluminium alloy (UNI 3571), $\bar{\sigma} = 574\ \bar{\epsilon}^{0.141}$ MPa, % r = 15, f = 0.075, R = 65 mm)

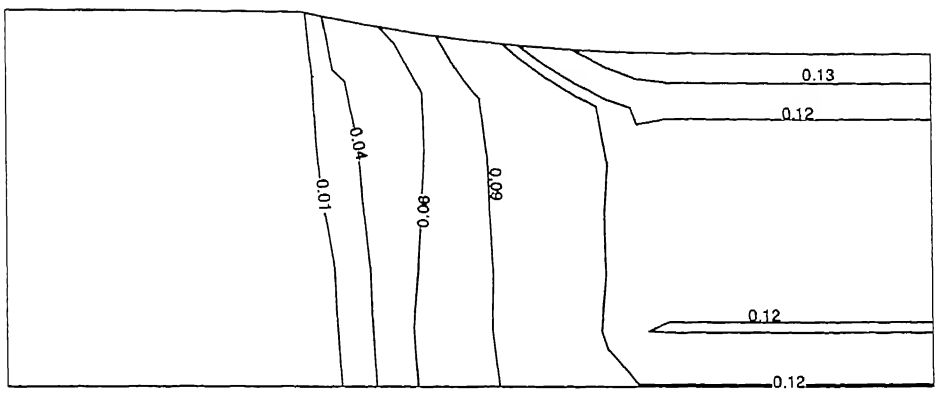

Figure 3.21: Damage distribution in plane strain rolling, Oyane's criterion [Oyane et al., 1980] (Material: aluminium alloy (UNI 3571), $\bar{\sigma} = 574\ \bar{\epsilon}^{0.141}$ MPa, % r = 10, f = 0.05, R = 65 mm)

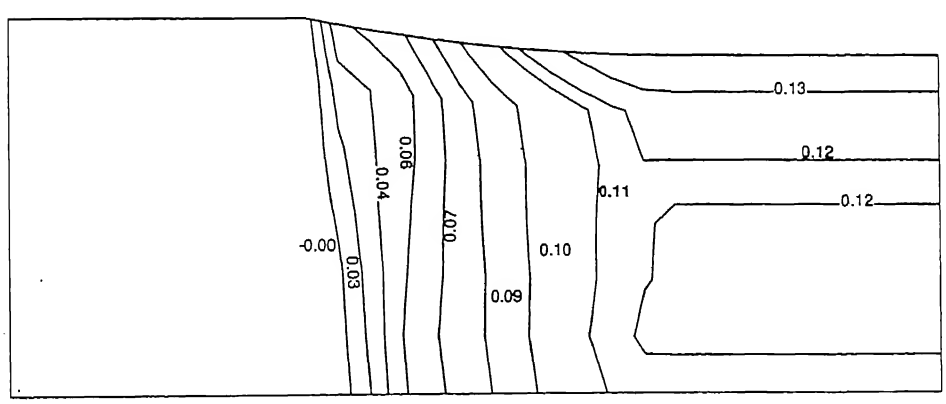

Figure 3.22: Damage distribution in plane strain rolling, Oyane's criterion [Oyane et al., 1980] (Material: aluminium alloy (UNI 3571), $\bar{\sigma} = 574\ \bar{\epsilon}^{0.141}$ MPa, % r = 10, f = 0.075, R = 130 mm)

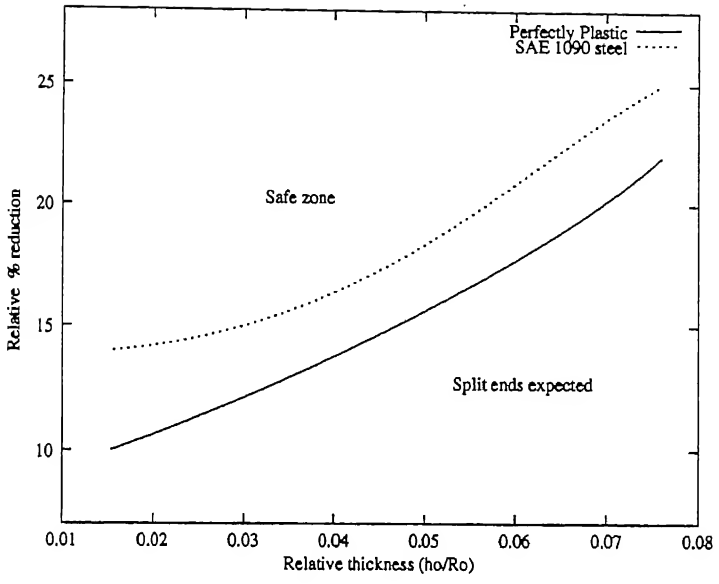

Figure 3.23: The boundary between safe and unsafe zones for perfectly plastic and strain hardening using HSC for split-ends [Material: SAE 1090 steel, $\bar{\sigma} = 1115\ \bar{\epsilon}^{0.19}$ MPa, R = 67 mm, f = 0.1]

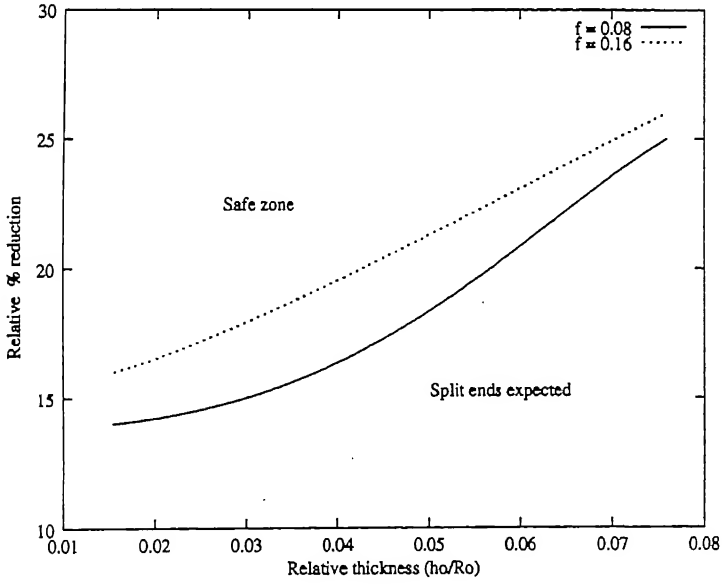

Figure 3.24: The boundary between safe and unsafe zones for different friction using HSC for split-ends [Material: SAE 1090 steel, $\bar{\sigma} = 1115\ \bar{\epsilon}^{0.19}$ MPa, R = 65 mm]

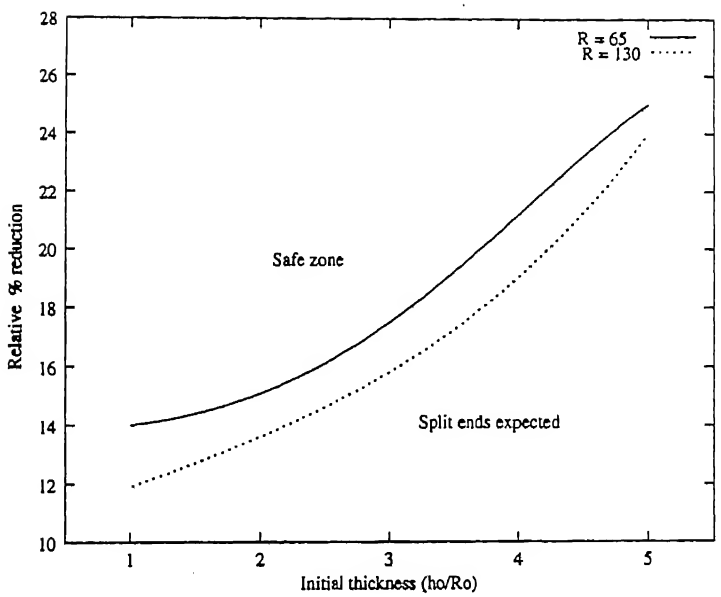

Figure 3.25: The boundary between safe and unsafe zones for different roll radius using HSC for split-ends [Material: SAE 1090 steel, $\bar{\sigma} = 1115\ \bar{\epsilon}^{0.19}$ MPa, f = 0.08]

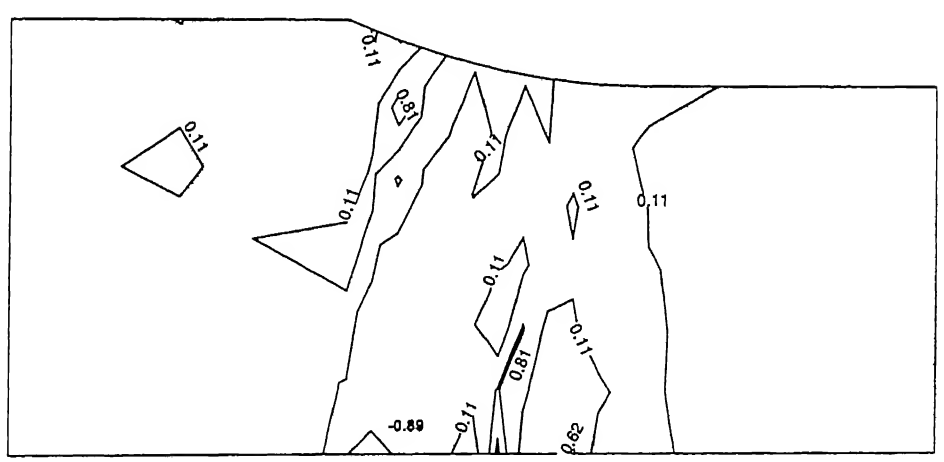

Figure 3.26: A typical hydrostatic stress distribution at split-end condition [Material: SAE 1090 steel, $\bar{\sigma} = 1115\ \bar{\epsilon}^{0.19}$ MPa, R = 65 mm at h_0 = 3 mm, f = 0.08]

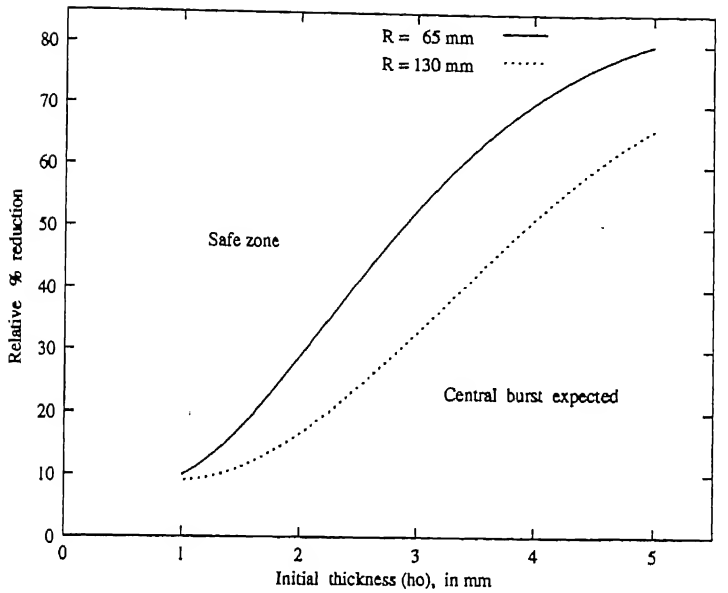

Figure 3.27: The boundary between safe and unsafe zones for different roll radius using HSC for central burst [Material: SAE 1090 steel, $\bar{\sigma} = 1115\ \bar{\epsilon}^{0.19}$ MPa, f = 0.08]

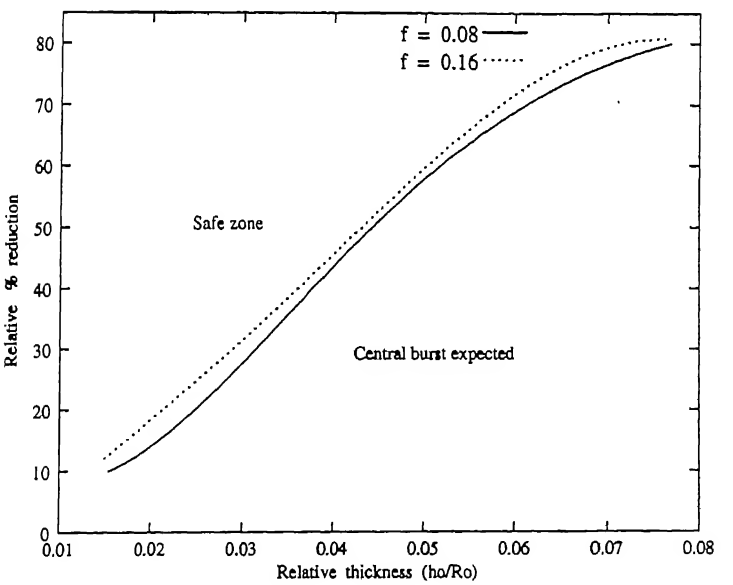

Figure 3.28: The boundary between safe and unsafe zones for different friction using HSC for central burst [Material: SAE 1090 steel, $\bar{\sigma} = 1115\ \bar{\epsilon}^{0.19}$ MPa, R = 65 mm]

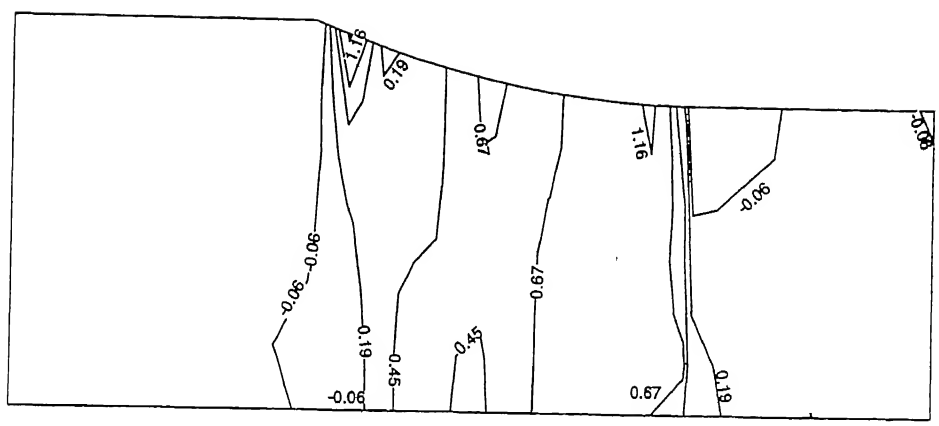

Figure 3.29: A typical hydrostatic stress distribution at central bursting condition (using HSC) [Material: SAE 1090 steel, $\bar{\sigma} = 1115\,\bar{\epsilon}^{0.19}$ MPa, $h_0 = 2$ mm, R = 65 mm, f = 0.08]

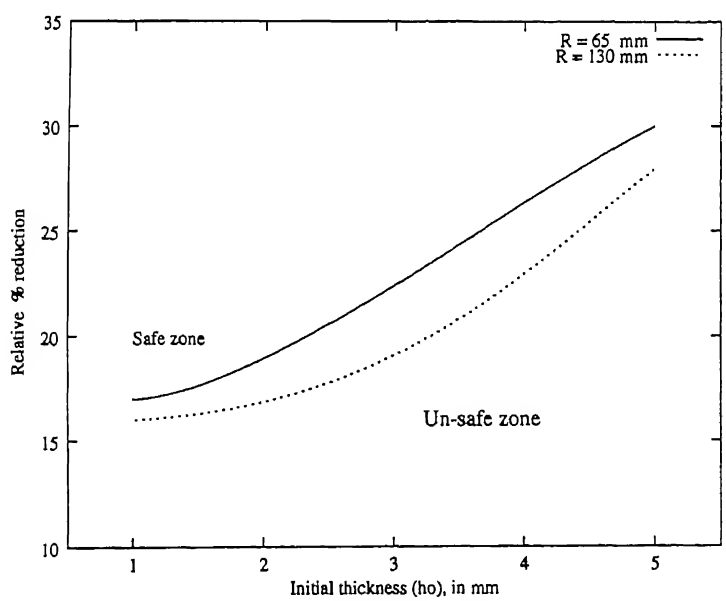

Figure 3.30: The boundary between safe and unsafe zones for different roll radius using critical damage criterion [Dhar et al., 1996] [Material: SAE 1090 steel, $\bar{\sigma} = 1115\,\bar{\epsilon}^{0.19}$ MPa, f = 0.08]

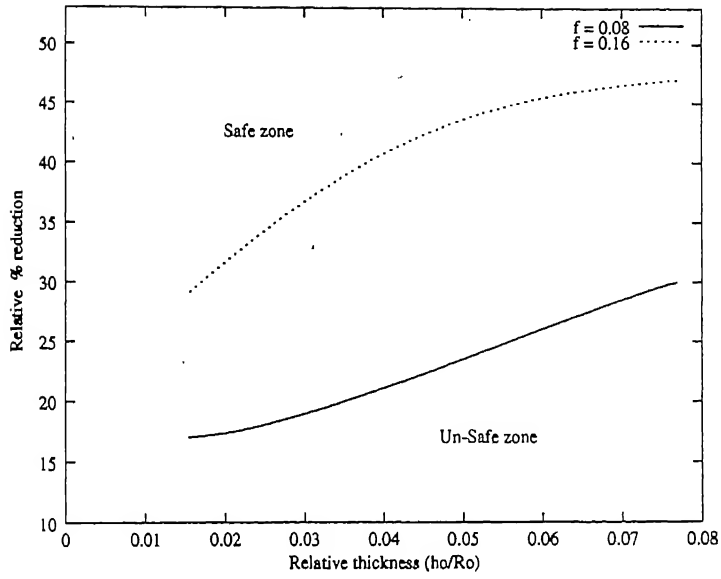

Figure 3.31: The boundary between safe and unsafe zones for different friction conditions using critical damage criterion [Dhar et al., 1996] [Material: SAE 1090 steel, $\bar{\sigma} = 1115\ \bar{\epsilon}^{0.19}$ MPa, R = 65 mm]

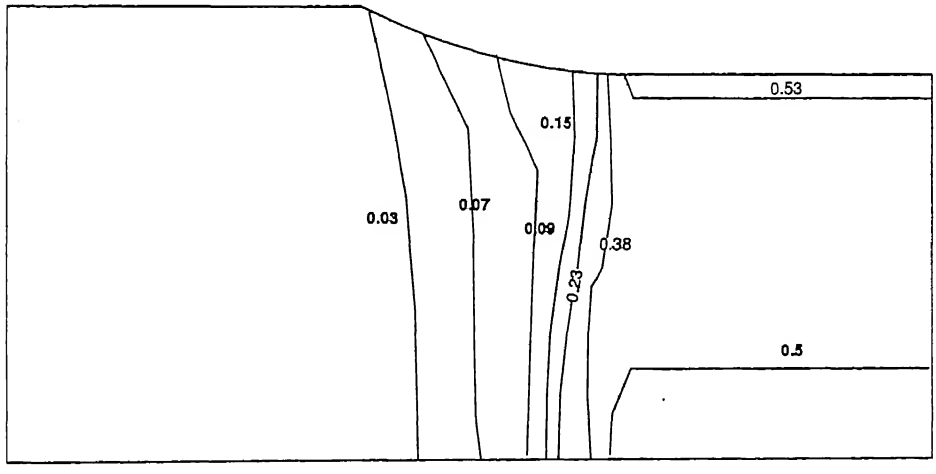

Figure 3.32: A typical hydrostatic stress distribution at central bursting condition (Dhar et al., 1996) [Material: SAE 1090 steel, $\bar{\sigma} = 1115\ \bar{\epsilon}^{0.19}$ MPa, $h_0 = 4$ mm, R = 65 mm, f = 0.08]

Chapter 4

Conclusions and Scope for Future Work

4.1 Conclusions

On the basis of results presented in chapter 3, the following conclusions are made.

- The present predictions of force, torque and pressure are in good agreement with the available experimental [Al-Salehi et al., 1973 and Shida and Awazuhara, 1973] and analytical [Dixit and Dixit, 1997] results.
- The present predictions based on hydrostatic stress criterion for split-ends are in good agreement with the available experimental [Turckzyn and Malinowski, 1996] results.
- Parametric study on the damage variable of critical damage criterion [Dhar et al., 1996] and Oyane's criterion [Oyane et al., 1980] shows that, damage distribution remains same but the value of damage variable is increasing with decrease in roll radius and increase in friction or reduction.
- Parametric study on the boundary between safe and unsafe zone is carried out to study the influence of process variables. It is observed that the safe zone is increasing with increase in roll radius or decrease in friction. The safe zone is higher for non-hardening material compared to the hardening material.
- It is observed that the predictions of HSC are more conservative than the critical damage criterion [Dhar et al., 1996].

4.2 Scope for the Future Work

In the present work, roll deformation, variation of coefficient of friction along the roll-work interface, effect front and back tensions are not considered and they can be included. To validate the fracture predictions made by the present work, experiments can be conducted.

References

Alberti, N., Barcellona, A., Masnata, A., and Micari, F., 1993, Central Bursting Defects in Drawing and Extrusion: Numerical and Ultrasonic Evaluation, *Annals of the CIRP*, **42** 269.

Al-Salehi, F.A.R., Firbank, T.C., and Lancaster, P.R., 1973, An Experimental Determination for the Roll Pressure Distribution in Cold Rolling, *International Journal of Mechanical Sciences*

Altan, T., and Knoerr, M., 1992, Application of the 2D Finite Element Method to Simulation of Cold Forging Processes, *Journal of Materials Processing Technology*, **33** 31.

Argon, A. S., and Im, J., 1975, Separation of Second Phase Particles in Spheroidised 1045 Steel, Cu 0.6,. Pct Cr Alloy and Maraging Steel in Plastic Straining, *Metallurgical Transactions - A*, **6** 839.

ASM handbook, Forming and Forging, 1988.

Avitzur, B., 1964, An Upper-Bound Approach to Cold-Strip Rolling, *ASME Journal of Engineering for Industry*, **86** 31.

Avitzur, B.,1980, *Metal Forming - The Application of Limit Analysis*, Marcel Dekker.

Avitzur, B., 1983, *Handbook of Metal Forming Processes*, John Wiley.

Avitzur, B., and Pachla, W., 1986, The Upper Bound Approach to Plane Strain Problems Using Linear and Rotational Velocity Fields -Part I: Basic Concepts, *ASME Journal of Engineering for Industry*, **108** 295.

Avitzur, B., and Pachla, W., 1986a, The Upper Bound Approach to Plane Strain Problems Using Linear and Rotational Velocity Fields -Part II: Applications, *ASME Journal of Engineering for Industry*, **108** 307.

Avitzur, B., Gordon, W., and Talbert, S., 1987, Analysis of Strip Rolling by the Upper Bound Approach, *Transactions of the ASME*, bf 109 338.

Avitzur, B., Van Tyne, C.J., Turckzyn, S., 1988, The Prevention of Central Bursts During Rolling, *ASME Journal of Engineering for Industry* **110** 173.

Berg, C.A., 1970, Plastic Dilation and Void Interaction, In: *Inelastic Behaviour of Solids* (Ed.M.F.Kanninen), McGraw-Hill.

Bland, D.R., and Ford, H., 1948, The Calculation of Roll Force and Torque in Cold Strip Rolling with Tensions, *Proceedings of Institute of Mechanical Engineers*, **159** 144.

Bland, D.R., and Sims, R.B., 1953, A Note on the Theory of Rolling with Tensions, *Proceedings of Institute of Mechanical Engineers*, **167** 371.

Bramley, A. N., and Osman, F. H., 1992, The Upper Bound Method, *Numerical Modeling of Material Deformation Processes - Research, Development and Applications* (Ed. P. Hartley et al.), Springer-Verlag, 114.

Bridgman, P. W., 1964, *Studies in Large Plastic Flow and Fracture*, Harvard University Press.

Clift, S. E., Hartley, P., Sturgess, C. E. N., and Rowe, G. W., 1990, Fracture Prediction in Plastic Deformation Processes, *International Journal of Mechanical Sciences*, **32** 1.

Cockcroft, M. G., and Latham, D. J., 1968, Ductility and the Workability of Metals, *Journal of the Institute of Metals*, **96** 33.

Collins, I. F., 1969, Slip-line Field for Compression and rolling with slipping friction, *International Journal of Mechanical Sciences*, **11** 971.

Cser, L., Geiger, M., Lange, K., Kals, J. A. G., and Hansel, M., 1993, Tool Life and Tool Quality in Bulk Metal Forming, *Proc. Inst. Mech. Engrs., Journal of Manufacture*, **207** 223.

Dawson, P. R., and Thompson, E. G., 1978, Finite Element Analysis of Steady-State Elasto-Viscoplastic Flow by the Initial Stress-Rate Method, *International Journal of Numerical Methods in Engineering*, **12** 47.

Dhar, S., 1995, A Continuum Damage Mechanics Model for Ductile Fracture, Ph.D Thesis, Indian Institute of Technology - Kanpur (India).

Dhar, S., Sethuraman, R., and Dixit, P. M., 1996, A Continuum Damage Mechanics Model for Void Growth and Micro-crack Initiation, *Engineering Fracture Mechanics*, **53** 917.

Dixit, U.S., 1997, *Cold flat rolling: Modelling with fuzzy parameters, anisotropic effects and residual stresses*, M.Tech., thesis, IIT kanpur

Dung, N. L., 1992a, Three Dimensional Void Growth in Plastic Materials, *Mechanics Research Communications*, **19** 227.

Dung, N. L., 1992b, Prediction of Void Growth in Tensile Test, *Mechanics Research Communications*, **19** 341.

Firbank, T.C., and Lancastar, P.R., 1965, A suggested slip line field for cold rolling with slipping friction, *International Journal of Mechanical Sciences*, **7** 847.

Freudenthal, A. M., 1950, *The Inelastic Behaviour of Solids*, John Wiley.

Goods, S. H., and Brown, C. M., 1979, The Nucleation of Cavities by Plastic Deformation, *Acta Metallurgica* **27**, 1.

Gurland, J., 1972, Observation on the Fracture of Cementite Particles in Spheroidised 1.05% C Steel Deformed at Room Temperature, *Acta Metallurgica*, **20**, 735.

Gurson, A. L., 1977, Continuum Theory of Ductile Rupture by Void Nucleation and Growth Part 1 - Yield Criteria and Flow Rules for Porous Ductile Media, *ASME Journal of Engineering Materials Technology*, **99** 2.

Hartley, P., Pillinger, P., and Sturgess, C. E. N., (Editors), 1992, *Numerical Modeling of Material Deformation Processes - Research, Development and Applications*, Springer-Verlag.

Herrmann, M., 1994, Extended Capabilities in Metal Forming Processes by New Interdisciplinary FEM Code, *Annals of the CIRP*, **43** 215.

Hill, R., 1950, *The Mathematical Theory of Plasticity*, Clarendon Press.

Hitchock, J.H., 1935, Roll nech bearings, *Transactions of ASME.*

Johnson, W., 1991, Manufacturing Defect Studies Noting Some of the Early Ideas of Rober Mallett (1810-1881), Irish Engineer - Scientist, *Journal of Material Processing Tecknology*, **26** 97.

Johnson, W., and Mamalis, A. G., 1977, A survey of Some Physical Defects Arising in Metal Working Processes, *Proc. 17th Int. MTDR Conf.,* Macmillan, 607.

Johnson, W., and Mellor, P. B., 1973, *Engineering Plasticity*, Von Nostsrand and Reinhold Company.

Karman, T. von, 1925, On the theory of rolling, *Z. Angew. Math. Mech.* **5** 139.

Knoerr, M., Lee, J., and Altan, T., 1992, Application of the 2D Finite Element Method to Simulation of Various Forming Processes, *Journal of Materials Processing Technology*, **33** 31.

Kudo, H., 1985 Upper bound Approach to Metal Forming Process to Date and in the Future, *Metal Forming and Impact Mechanics* (Ed. S. R. Reid), Pergamon.

Le Roy, G., Embury, J. D., Edward, G., and Ashby, M. F., 1981, A Model of Ductile Fracture Based on the Nucleation and Growth of Voids, *Acta Metallurgica*, **29** 1509.

Lee, E. H., and McMeeking, R. M., 1978, Cocerning the Analysis of Ceentral Burst in Metal Forming, *ASME journal of Engineering for Industry*, **100** 386.

Lemaitre, J., 1985, A Continuous Damage Mechanics Model for Ductile Fracture, *ASME Journal of Engineering Materials and Technology*, **107** 83.

Li, G.J., and Kobayashi, S., 1982, Rigid Plastic Finite Element Analysis of Plane Strain Rolling, *ASME Journal of Engineering for Industry*, **104** 55.

Lin, C.C.Y., and Atkinson, M., 1996, Comparison of three cold mill rolling force models, *2d Int. Conf. on Modelling Of Metal Rolling Processes*, 478.

Malinowski, Z., 1993, Elastoplastic Finite Element Solution to the Stress Problem in the Plane-Strain Cold Rolling Process, *Metallurgy and Foundry Engineering*, **19** 323.

Malinowski, Z., and Lenard, J. G., 1993, Experimental Substantiation of an Elasto-plastic Finite Element Scheme for Flat Rolling, *Computer Methods in Applied Mechanics and Engineering*, **104** 1.

Mamalis, A. G., and Johnson, W., 1987, Defect in the Processing of Metals and Composites, *Computational Methods for Predicitng Material Processing Defects* (Ed. M. Predeleanu), Elservier, 231.

Maniatty, A. M., 1994, Predicting Residual Stresses in Steady State Forming Processes, *Computing Systems in Engineering*, **5** 171.

Maniatty, A. M., Dawson, P. R., and Weber, G. G., 1991, An Eulerian Elasto-Viscoplastic Formulation for Steady-State Forming Processes, *International Journal of Mechanical Sciences*, **33** 361.

McClintock, F. A., 1968, A Criterion for Ductile Fracture by the Growth of Holes, *ASME Journal of Applied Mechanics*, **90**, 363.

Mori, K., Osakada, K and Oda, T., 1982, Simulation of plane strain rolling by rigid-plastic finite element method, Extrusion and Drawing, *International Journal of Mechanical Sciences*, **24**, 519.

Needleman, A., and Tvergaard, V., 1984, An Analysis of Ductile Rupture in Notched Bars, *Journal of the Mechanics and Physics of Solids*, **32** 461.

Norris, D. M., Reaugh, J. E., Moran, B., and Quinnones, D. F., 1978, A Plastic Strain Mean Stress Criterion for Ductile Fracture, *ASME Journal of Engineering Materials Technology*, **100**, 279.

Oh, S. I., Chen, C. C., and Kobayashi, S., 1979, Ductile Fracture in Axisymmetric Extrusion and drawing. Part 2: Workability in Extrusion and Drawing, *ASME Journal of Engineering for Industry*, **101** 36.

Orowan, E., 1943, The calulation of roll Pressure in hot and cold frat rolling, *Proceedings of Institute of Mechanical Engineers*, **150** 147.

Oyane, M., 1972, Criteria of Ductile Strain, *Bulletin of JSME*, **15** 1507.

Oyane, M., Sato, T., Okimoto, K., and Shima, S., 1980, Criteria for Ductile Fracture and their Applications, *Journal of Mechanical Working Technology*, **4**, 65.

Petrzyk, M., and Lenard, J.G., 1991, Thermal-Mechanical Modelling of Flat Rolling Processes, *Springer-Vverlag.*

Prakash, R.S., Dixit, P.M. and Lal, G.K., Steady-state plane strain cold rolling of a strain-hardening material, *Journal of Materials Processing Technology*, **52** 338.

Reddy, J. N., 1993, *An Introduction to the Finite Element Method*, McGraw-Hill.

Reddy, N. V., Dixit, P.M. and Lal, G. K., 1996, Central bursting and optimal die profile for axisymmetric extrusion, *ASME Journal of Manufacturing Science and Engineering*, **118** 579.

Rice, J. R., and Tracey, D. M., 1969, On the Ductile Enlargement of Voids in Triaxial Stress Field, *Journal of the Mechanics and Physics of Solids*, **17** 201.

Roy Choudhuri, R., and Lenard, J.G., 1984, A mathematical model of cold rolling experimental substantation, *Proc. 1st Int. Conf. Tech. Plast., Tokyo*, 1138.

Shida, S., and Awazuhara, H., 1973, Rolling load and torque in cold rolling, *J. Japan Soc. Tech. Plast.*, **14** 267.

Shimazaki, Y., and Thompson, E. G., 1981, Elasto-Viscoplastic Flow with Special Attention to Boundary Conditions, *International Journal of Numerical Methods in Engineering*, **17** 97.

Stone, M.D., 1953, Rolling of thin strips - part 1, *Iron And Steel Eng Year Book.*

Surya Narayana, G., 1998, A Set-up Model for Tandem Cold Rolling Mill, *M.Tech. thesis*, IIT Bombay.

Thomason, P. F., 1990, *Ductile Fracture of Metals*, Pergamon.

Thompson, E. G., and Berman, H. M., 1984, Steady-State Analysis of Elasto-Viscoplastic Flow During Rolling, *Numerical Analysis of Forming Processes* (Eds. J. F. T. Pittman et al.), John Wiley, 269.

Thompson, E. G., and Yu, S., 1990, A Flow Formulation for Rate Equilibrium Equations, *International Journal of Numerical Methods in Engineering*, **30** 1632.

Thomsen, E. G., Yang, C. T., and Kobayashi, S., 1965, *Mechanics of plastic Deformation in Metal Processing*, Macmillan.

Turckzyn, S., and Malinowski, Z., 1996, Split ends and central burst defects in rolling, *Materials Processing Defects*, (Eds. S.K.Ghosh and M.Predeleanu), Elsevier, 401.

Tselikov, A.I., 1939, The influence of external friction and tension on roll face pressure, *Metallurgy*, **6** 61.

Tseng, A.A., Wang, R., and Lau, A.C., 1998, Local variations of strain rate in roll bite region during rolling of steels, *Journal of Engineering Materials Tecknology*, **120** 86.

Tvergaard, V., 1981, Influence of Voids on Shear Band Instabilities Under Plane Strain Conditions, *International Journal of Fracture*, **17** 389.

Zhu, Y.D., Avitzur, B., 1988, Criteria for the Prediction of Split Ends, *Transactions of ASME*, **110** 162.

Zienkiewicz, O. C., 1984, Flow Formulation for Numerical Solution of Forming Processes, *Numerical Analysis of Forming Processes* (Eds. J. F. T. Pittman et al.), John Wiley, 1.

Zienkiewicz, O. C., Jain, P. C., and Onate, E., 1978, Flow of Solids During Forming and Extrusion: Some Aspects of Numerical Solutions, *International Journal of Solids and Structures*, **14** 15.